# Interacting instanton liquid in QCD at zero and finite temperatures

T. Schäfer* and E. V. Shuryak
*Department of Physics, State University of New York at Stony Brook, Stony Brook, New York 11794*
(Received 25 September 1995)

In this paper we study the statistical mechanics of the instanton liquid in QCD. After introducing the partition function as well as the gauge-field- and quark-induced interactions between instantons, we describe a method to calculate the free energy of the instanton system. We use this method to determine the equilibrium density and the equation of state from numerical simulations of the instanton ensemble in QCD for various numbers of flavors. We find that there is a critical number of flavors above which chiral symmetry is restored in the ground state. In the physical case of two light and one intermediate mass flavors, the system undergoes a chiral phase transition at $T \simeq 125$ MeV. We show that the mechanism for this transition is a rearrangement of the instanton liquid, going from a disordered, random phase at low temperatures to a strongly correlated, molecular phase at high temperature. We also study the behavior of mesonic susceptibilities near the phase transition.

PACS number(s): 12.38.Lg, 05.70.−a, 11.30.Rd

## I. INTRODUCTION

Understanding the vacuum structure of gauge theories such as QCD is one of the main problems in quantum field theory today. It also provides the theoretical foundation for hadronic models and hadronic phenomenology from the underlying field theory of the strong interaction, quantum chromodynamics. There are a number of indications that instantons, classical tunneling trajectories in imaginary (Euclidean) time, are an important ingredient of the QCD vacuum.

Soon after the discovery of instantons 20 years ago [1], it became clear that instantons may provide at least a qualitative understanding of many features of the QCD vacuum. Instantons solve the $U(1)_A$ problem [2], they give a mechanism for chiral symmetry breaking [3], contribute to the gluon condensates, and lead to a nonperturbative vacuum energy [4,5].

The development of a quantitative theory based on these ideas took much longer. The instanton liquid model was originally suggested by Shuryak in 1982 [6], guided mainly by phenomenological considerations. Later, Diakonov and Petrov developed an analytical approach based on the variational method [7] (see also [8]). The first numerical simulations of the ''instanton liquid'' were reported in [9,10]. During the past two years, we have shown [11–13] that the ''random instanton liquid model'' (RILM) provides a successful description of a large number of hadronic correlation functions, including mesons and baryon made of light quarks, heavy-light systems, and glueballs. These correlators not only give reasonable values for the corresponding resonance masses and coupling constants, but they also compare well with point-to-point correlation functions extracted from phenomenology [14] or measured on the lattice [15].

Following these developments, several recent lattice simulations have focused on the role of instantons in the QCD vacuum, both at zero and finite temperatures. Using a method called ''cooling,'' one can relax any given gauge-field configuration to the closest classical component of the QCD vacuum. The resulting configurations were known to be of multi-instanton type [16], but the more recent work by Chu *et al.* [17] has provided quantitative measurements of the parameters of the instanton liquid, as well as detailed studies of the dynamical effects of instantons. These authors conclude that the instanton density in the quenched theory (without dynamical fermions) at zero temperature is $n \simeq (1.3\text{–}1.6)\ \mathrm{fm}^{-4}$ while the average size is about $\rho \simeq 0.35$ fm. These numbers confirm the key parameters $n = 1\ \mathrm{fm}^{-4}$ and $\rho = 1/3$ fm of the instanton liquid model mentioned above. In addition to that, Chu *et al.* studied correlation functions in the cooled configurations, finding that they hardly change from the original, fully quantum configurations. This would imply that instanton effects dominate over perturbative and confinement forces in determining the structure of low-lying hadronic states. A lattice measurement of the instanton size distribution for pure SU(2) gauge theory was performed in [18], where also an attempt was made to study correlations between instantons. The size distribution was compared to the predictions of the interacting instanton liquid model in [19].

In this paper we want to report a detailed study of the statistical mechanics of the interacting instanton liquid model (IILM), both at zero and finite temperatures. The purpose of this study is twofold. First, we want to give a fully consistent treatment of the model at zero temperature. Our goal is to construct an interacting instanton ensemble that is consistent with the low energy theorems that follow from the renormalization and symmetry properties of QCD, such as the trace anomaly, chiral Ward identities, or Ward identities for fluctuations of the topological charge. Second, we explore the model at nonzero temperature. In this paper, we will limit ourselves to the analysis of bulk properties, such as the energy density, the chiral condensate, and mesonic susceptibilities. A detailed study of hadronic correlation functions will be presented in a forthcoming publication [20].

At zero temperature, we want to study the importance of instanton interactions and determine those features of the in-

*Present address: Institute for Nuclear Theory, University of Washington, Seattle, WA 98195.

 

teracting ensemble that differ from the simplest, random ensemble (RILM). We also want to determine the relation between the instanton interaction and global parameters (such as the density and average size) of the instanton liquid. Furthermore, we want to quantify the role of instanton interactions in producing correlations among the instantons. This is of interest, since despite the success of the random model in the description of most hadronic correlation functions [11], it fails in channels where the single instanton interaction is strongly repulsive (such as the $\eta'$ and $\delta$ meson channels). As shown in [21,13,22], the correlations among instantons caused by their classical and fermion-induced interactions lead to a correct description of topological charge screening and the $\eta'$ channel.

The role of correlations among the instantons is particularly important with regard to the nature of the chiral phase transition. Originally, it was believed [6,23,24] that chiral symmetry is restored because of the rapid disappearance of instantons at high temperature [25]. Ilgenfritz and Shuryak realized [26] that instantons can be present even above the chiral phase transition, as strongly correlated instanton–anti-instanton molecules (see also [27]). In this case, the transition is determined by the phase equilibrium between the low temperature ''liquid'' and high temperature ''molecular'' phase. Shuryak and Velkovsky later argued that instanton suppression is essentially a plasma effect and should not be present below the phase transition [28]. This means that the transition is driven by the formation of molecules [31,32], rather than by the suppression of individual instantons. There is some support for this scenario from lattice simulations performed by Chu and Schramm [29]. Extending the cooling method to finite temperature, they find that the instanton density is essentially independent of temperature below the phase transition, while it is exponentially suppressed above the transition temperature. First evidence for the presence of molecules near $T_c$ was reported in [30].

So far, the transition has only been studied using the schematic ''cocktail'' model introduced by Ilgenfritz and Shuryak [31]. In this model, the instanton liquid consists of two components, a random and a molecular one. The free energy is determined separately for the two components and their concentrations are then determined by minimizing the total free energy. The chiral phase transition occurs when the concentration of random instantons is zero. This approach predicts the presence of a substantial number of instantons even if $T>T_c$, causing new nonperturbative effects in the plasma phase. One such effect, studied in [32], is the ''molecule-induced'' effective interaction between quarks, leading to a spectrum of spacelike screening masses consistent with lattice data. Another possible consequence, the survival of certain hadronic modes above the phase transition was studied in [33].

In the present work, we significantly improve on the schematic model used before and do a complete calculation in the interacting ensemble. In this way, many approximations are relaxed and all possible correlations among instantons (not just polarized instanton–anti-instanton pairs) are included. The paper is organized as follows. In Sec. II we introduce the partition function of the instanton liquid and specify the gauge field and fermion-induced interactions between instantons. Detailed parametrizations of these interactions can be found in the appendices. In Sec. III we describe the method which is used to calculate the partition function. In Sec. IV we use this method to study the instanton ensemble at zero temperature. In Secs. V and VI, we generalize the method to finite temperature and study the nature of the chiral phase transition in the instanton liquid. In Sec. VII we study some phenomena associated with the transition, in particular, the Dirac spectrum and the mesonic susceptibilities.

## II. THE PARTITION FUNCTION OF THE INSTANTON LIQUID

The Euclidean partition function of QCD is given by

$$Z=\int DA_\mu \exp(-S[A_\mu])\prod_f^{N_f}\det(i\hat{D}+im_f), \tag{1}$$

where the gauge-field action is given by $S[A_\mu]=\frac{1}{4}\int d^4x \mathrm{Tr}(F_{\mu\nu}F_{\mu\nu})$ and the Dirac operator is defined by $\hat{D}\psi=\gamma_\mu(\partial_\mu-iA_\mu)\psi$.

The main assumption underlying the instanton model is that the full partition function can be approximated by a partition sum in which the relevant gauge configurations are superpositions of instantons and anti-instantons. In this partition function, the relevant degrees of freedom are the collective coordinates associated with $N_+$ instantons and $N_-$ anti-instantons:

$$Z=\frac{1}{N_+!N_-!}\int\prod_i^{N_++N_-}[d\Omega_i d(\rho_i)]\exp(-S_{\mathrm{int}})\times\prod_i^{N_f}\det(i\hat{D}+im_f). \tag{2}$$

Here, $d\Omega_i=dU_i d^4z_i d\rho_i$ is the measure in the space of collective coordinates, color orientation, position, and size, associated with single instantons. For the gauge group $\mathrm{SU}(N_c)$, there are $4N_c$ collective coordinates per instanton. Fluctuations around individual instantons are included in Gaussian approximation. This gives the semiclassical instanton amplitude, originally calculated by 't Hooft [2]. To two-loop accuracy, it reads

$$d(\rho)=C_{N_c}\rho^{-5}\beta_1(\rho)^{2N_c}\exp\left[-\beta_2(\rho)+\left(2N_c-\frac{b'}{2b}\right)\frac{b'}{2b}\frac{1}{\beta_1(\rho)}\ln[\beta_1(\rho)]\right], \tag{3}$$

$$C_{N_c}=\frac{4.6\exp(-1.86N_c)}{\pi^2(N_c-1)!(N_c-2)!}, \tag{4}$$

where $\beta_1(\rho)$ and $\beta_2(\rho)$ are the one- and two-loop beta functions,

$$\beta_1(\rho)=-b\ln(\rho\Lambda),$$

$$\beta_2(\rho)=\beta_1(\rho)+\frac{b'}{2b}\ln\left(\frac{2}{b}\beta_1(\rho)\right), \tag{5}$$

with the one- and two-loop coefficients

$$b=\frac{11}{3}N_c-\frac{2}{3}N_f, \quad b'=\frac{34}{3}N_c^2-\frac{13}{3}N_cN_f+\frac{N_f}{N_c}. \quad (6)$$

The coefficient $C_{N_c}$ was calculated in a Pauli-Villars renormalization scheme and $\Lambda$ is the corresponding scale parameter. The classical action $S_0=8\pi^2/g^2$ is included in the semiclassical amplitude (3). The classical interaction between instantons is denoted by $S_{\rm int}$. We approximate this interaction by a pure two-body interaction $S_{\rm int}=\frac{1}{2}\Sigma_{I\neq J}S_{\rm int}(\Omega_{IJ})$ which only depends on the relative coordinates of the two instantons. The importance of genuine three-body effects in the classical interaction between instantons was studied in [9], with the conclusion that this contribution is negligible as long as the density is not extremely large.

The two-body interaction $S_{\rm int}(\Omega_{IJ})=S[A_\mu(\Omega_{IJ})]-2S_0$ is calculated classically, by inserting the two-instanton gauge potential $A_\mu(\Omega_{IJ})$ into the action. There are no exact instanton–anti-instanton solutions to the classical Yang-Mills equations, so in practice one has to use an ansatz for the gauge potential. The resulting interaction will then depend on the details of the trial function. Various trial functions have been used in the literature: (i) the sum *Ansatz* [7], (ii) the ratio *Ansatz* [9], (iii) the conformally invariant Yung *Ansatz* [34], and (iv) the exact streamline (or valley) solution [35]. The latter is characterized by the fact that the action is minimized in all directions except along the collective coordinate describing the separation between the two instantons. In this sense, the streamline solution is the optimal classical instanton–anti-instanton configuration.

In order to discuss the properties of the classical interaction between instantons, let us introduce the four-vector $u_\mu=1/2i\ {\rm tr}(U_I^\dagger U_A\tau_\mu^+)$, where $U_{I,A}$ are the orientation matrices of the instanton and anti-instanton and $\tau_\mu^+$ is the $2\times 2$ matrix $(\vec{\tau},-i)$. For the gauge-group SU(2), $u_\mu$ is a real unit vector whereas for SU(3) it is a complex vector with $|u|^2\leq 1$. In any case, we can define an angle $\theta$ by

$$\cos\theta=\frac{|u\cdot\hat{R}|}{|u|}, \quad (7)$$

where $R=z_I-z_A$ is the vector connecting the centers of the two instantons. For all the trial functions mentioned above, the large distance part of the instanton–anti-instanton interaction is given by

$$S_{\rm int}=\beta_1(\overline{\rho})\frac{4\rho_1^2\rho_2^2}{R^4}|u|^2(1-4\ \cos^2\theta), \quad (8)$$

which is the dipole-dipole interaction originally discussed by Callan, Dashen, and Gross [3]. The interaction is given in units of the single instanton action $\beta_1(\rho)$. The argument of the beta function is not exactly determined without a calculation of the fluctuations around the two-instanton configuration. In practice, we take the argument to be the geometric mean $\overline{\rho}=\sqrt{\rho_I\rho_A}$ of the two instanton radii. The interaction is attractive for the relative orientation $\cos\theta=1$, but vanishes after averaging over all angles $\theta$. The short distance behavior depends on the ansatz chosen. In the sum *Ansatz*, there is a substantial repulsive core at distances $R<\sqrt{6}\rho$ [7], but the amount of repulsion at short distances becomes significantly weaker using the more refined trial functions. We will discuss this question in more detail in the next section. A parametrization of the interaction in the ratio and streamline *Ansätz* is given in Appendix A. In Fig. 1(a) we show the ratio and streamline interaction for the most attractive and repulsive orientations. One clearly observes that the interactions are similar at large distance, but differ significantly at short distance. In particular, the streamline interaction has no repulsion at all for the most attractive orientation. The interaction smoothly approaches $S_{\rm int}=-2S_0$ at short distance, corresponding to the annihilation of the instanton–anti-instanton pair. Figure 1(a) also shows the effect of a phenomenological core in the streamline interaction. The reasoning behind this modification will be discussed in more detail in the next section.

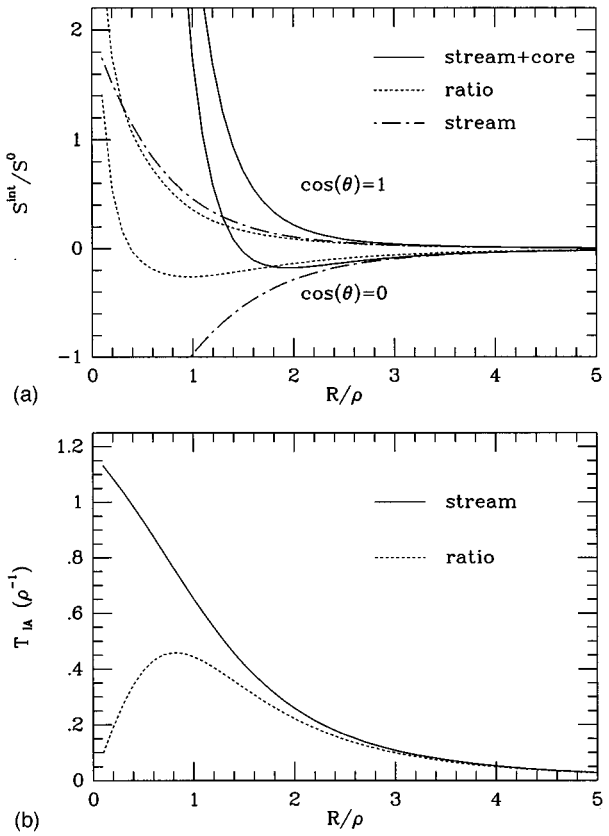


FIG. 1. (a) Classical instanton–anti-instanton interaction in the streamline (dash-dotted line) and ratio *Ansatz* (short dashed line). The interaction is given in units of the single instanton action $S_0$ for the most attractive ($\cos\theta=1$) and most repulsive ($\cos\theta=0$) orientations. The dash-dotted curves show the original streamline interaction, while the solid curves show the interaction including the core introduced in Sec. III. (b) shows the fermonic overlap matrix elements in the streamline (solid curve) and ratio *Ansatz* (dashed curve). The matrix elements are given in units of geometric mean of the instanton radii.

For all the trial functions except for the simple sum *Ansatz*, the instanton-instanton interaction is much weaker than the instanton–anti-instanton one. In fact, in the streamline *Ansatz*, the instanton-instanton interaction vanishes. This is a reflection of the fact that there is an exact two-instanton solution (with $S=2S_0$) for arbitrary values of the relative coordinates.

The fermionic determinant induces a very nonlocal interaction among the instantons. Evaluating this determinant exactly in the instanton ensemble still constitutes a formidable problem. In practice, we factorize the determinant into a low and a high momentum part [36],

$$\det(\hat{D}+m_f)=\left(\prod_i^{N_++N_-} 1.34\rho_i\right)\det(T+im_f), \tag{9}$$

where the first factor, the high momentum part, is the product of contributions from individual instantons calculated in Gaussian approximation, whereas the low momentum part associated with the fermionic zero modes of individual instantons is calculated exactly.

This means that the instanton-induced 't Hooft interaction between quarks [2,37] is included in all orders. The low momentum part of the spectrum of the Dirac operator is also of special significance in connection with the structure of chiral symmetry breaking. $T_{IA}$ is the $N_+\times N_-$ matrix of overlap matrix elements:

$$T_{IA}=\int d^4x\,\phi^\dagger_{A0}(x-z_A)i\hat{D}_x\phi_{I0}(x-z_I), \tag{10}$$

where $\phi_{I,A0}$ are the fermionic zero mode wave functions of the instanton and anti-instanton. Because of the chirality of the zero modes, the fermionic overlap matrix elements between instantons with the same topological charge vanishes. In the following, we will only consider quadratic matrices with $N_+=N_-$. This means that we study the system at fixed topological charge $Q=N_+-N=0$, rather than at fixed theta angle. In the thermodynamic limit, the distribution of winding numbers is sharply peaked around zero [38], and fixing the total topological charge is not expected to affect our results. Fluctuations of the topological charge are important in connection with the $U(1)_A$ problem. They can be studied by considering appropriately chosen subsystems [21]. We find that local fluctuations obey the expected Ward identities and that the mass of the $\eta'$ has the correct value.

The general structure of the overlap matrix elements is given by $T_{IA}=(u\cdot R)f(R)$. This means that, like the gauge-field-induced interaction, the fermionic overlap is maximal when the relative instanton–anti-instanton orientation is given by $\cos\theta=1$. Similar to the gauge-field-induced interaction between instantons, the fermionic overlap matrix elements depend on the *Ansatz* for the two-instanton gauge potential. In this case, however, the dependence on the trial function is not as important. For the sum *Ansatz*, one can use the equations of motion and replace the covariant derivative in (10) by an ordinary one. The result can be parametrized by

$$T_{IA}=i(u\cdot R)\frac{1}{\rho_I\rho_A}\frac{4.0}{(2.0+R^2/\rho_I\rho_A)^2}, \tag{11}$$

which is exact at large distances. The streamline *Ansatz* gives the same large distance behavior, but differs at small separations. As long as the instanton ensemble is sufficiently dilute, this difference does not strongly affect physical observables. We give a parametrization of the streamline matrix elements in Appendix B.

## III. THE FREE ENERGY OF THE INSTANTON ENSEMBLE

In this section, we describe a method to evaluate the partition function of the instanton liquid. Using this method, we can calculate the free energy numerically as a function of the density of instantons, and determine the equilibrium density from the condition that the free energy is minimal.

The problem in determining the free energy is connected with the fact that the complicated statistical mechanics associated with the partition function (2) can, in general, only be dealt with by performing Monte Carlo simulations [9,10,39]. These simulations are ideally suited for the calculation of various expectation values, but do not give a direct determination of the partition function, which provides the overall normalization. Previous Monte Carlo calculations have therefore been restricted to simulations of the ensemble at a fixed density of instantons, which was determined from phenomenological considerations (typically 1 $\mathrm{fm}^{-4}$). Here, we want to go beyond this approximation and minimize the free energy. A method to calculate the partition sum, which is well known in statistical mechanics, quantum mechanics (see, e.g., [40]), and lattice gauge theory [41], is ''adiabatic switching.'' For this purpose, one writes the effective action as

$$S_{\mathrm{eff}}=S_0+\alpha S_1, \tag{12}$$

which interpolates between a solvable action $S_0$ and the full action $S_0+S_1$. If the partition function for the system governed by the action $S_0$ is known, the full partition function can be determined from

$$\ln Z(\alpha=1)=\ln Z(\alpha=0)-\int_0^1 d\alpha'\langle 0|S_1|0\rangle_{\alpha'}, \tag{13}$$

where the expectation value $\langle 0|\cdot|0\rangle_\alpha$ depends on the coupling constant $\alpha$. In our case, the effective action is given by

$$S_{\mathrm{eff}}=-\sum_{i=1}^{N_++N_-}\ln[d(\rho_i)]+S_{\mathrm{int}}+\mathrm{tr}\,\ln(i\hat{D}+im_f). \tag{14}$$

The obvious choice for decomposing the effective action of the instanton liquid would be to identify the logarithm of the single instanton distribution with the free action, $S_0=\Sigma_i\ln[d(\rho_i)]$. This procedure, however, does not work since the instanton distribution behaves like $d(\rho)\sim\rho^{(b-5)}$, so that the $\rho$ integration in the free partition function would not be convergent. This is the famous infrared problem which plagues the dilute instanton gas approximation [3]. As explained in more detail in the next section, the instanton liquid is stabilized by the repulsive core in the gauge field interaction once the full interaction is taken into account. We therefore consider the decomposition

$$S_{\mathrm{eff}}=\sum_{i=1}^{N_++N_-}\left(-\ln[d(\rho_i)]+(1-\alpha)\nu\frac{\rho_i^2}{\overline{\rho^2}}\right)+\alpha(S_{\mathrm{int}}+\mathrm{tr}\,\ln(i\hat{D}+im_f)), \tag{15}$$

where $\nu=(b-4)/2$ and $\overline{\rho^2}$ is the average size squared of the instantons with the full interaction included. The term pro-

portional to $(1-\alpha)$ serves to regularize the $\rho$ integration for $\alpha=0$. It disappears for $\alpha=1$, where the original action is recovered. The specific form of this term is irrelevant; our choice here is motivated by the fact that [at least for the one-loop measure $d(\rho)$] $S_{\rm eff}(\alpha=0)$ yields a single instanton distribution with the correct average size $\overline{\rho^2}$. This means that the single instanton distribution generated by $S_{\rm eff}(\alpha=0)$ is a variational *Ansatz* for the full one-instanton distribution.

The partition function corresponding to the variational single instanton distribution is given by

$$Z_0=\frac{1}{N_+!N_-!}(V\mu_0)^{N_++N_-},$$

$$\mu_0=\int_0^\infty d\rho d(\rho)\exp\left(-\nu\frac{\rho^2}{\overline{\rho^2}}\right), \tag{16}$$

where $\mu_0$ is the normalization of the one-body distribution. The $\rho$ integration in $\mu_0$ is regularized by the second term in (15). The full partition function obtained from integrating over the coupling $\alpha$ is

$$\ln Z=\ln(Z_0)+N\int_0^1 d\alpha'\langle 0|\,\nu\frac{\rho^2}{\overline{\rho^2}}$$

$$-\frac{1}{N}[S_{\rm int}+{\rm tr}\,\ln(i\hat{D}+im_f)]|0\rangle_{\alpha'}, \tag{17}$$

where $N=N_++N_-$. The free energy density is finally given by $F=-1/V\,\ln Z$ where $V$ is the four-volume of the system. The pressure and the energy density are related to $F$ by

$$p=-F,\quad \epsilon=T\frac{dp}{dT}-p. \tag{18}$$

At zero temperature, we have $\epsilon=-p=F$ and the free energy determines the shift of the QCD ground state relative to the perturbative vacuum. Such a shift is certainly present in our case, since tunneling lowers the ground state energy.

The full partition function can be compared to the variational *Ansatz* introduced in [7] and employed in many works on the subject [42,23,26,24,35,31]. For simplicity, we restrict the discussion at this point to pure gauge theory, i.e., neglect the fermionic determinant. Since the variational *Ansatz* ignores any correlation between instantons, only the color and spatial average of the interaction enters

$$\int d^4RdU\; S_{\rm int}(R,U,\rho_1,\rho_2)=\kappa^2\frac{N_c}{N_c^2-1}\rho_1^2\rho_2^2, \tag{19}$$

where $S_{\rm int}(R,U,\rho_1,\rho_2)$ is the interaction of two instantons with radii $\rho_{1,2}$, separation $R$, and relative orientation $U$. In the sum *Ansatz*, both the $II$ and $IA$ interactions give the same average repulsion $\kappa^2=\frac{27}{4}\pi^2$ [7]. In the ratio and streamline *Ansatz*, this repulsion is considerably weaker. In the streamline *Ansatz*, only the $IA$ interaction is repulsive with $\kappa^2=4.772$ [35].

If the variational single instanton distribution $d(\rho)\exp(-\nu\rho^2/\overline{\rho^2})$ is close to the true distribution for $\alpha=1$, we can calculate the expectation value in (17) using the variational one. One finds $\langle S_{\rm int}\rangle\simeq\langle S_{\rm int}\rangle_{\alpha=0}=N\nu/2$ and the resulting estimate for the partition function is

$$Z=\frac{1}{[(N/2)!]^2}(V\mu_0)^N\exp\left(-\frac{N\nu}{2}\right), \tag{20}$$

which agrees with the result derived in [7]. Varying $F=-1/V\,\ln Z$ with respect to the density, one finds the expected result $N/V=2\mu_0$.

Numerical results for different interactions were compared in [42,35]. For the sum *Ansatz*, the variational method gives $N/V=0.18\Lambda^4$ with $\overline{\rho}=0.48\Lambda^{-1}$, whereas the streamline *Ansatz* gives $N/V=0.54\Lambda^4$ and $\overline{\rho}=0.69\Lambda^{-1}$. The dimensionless diluteness $f=0.5\pi^2\rho^4(N/V)$ (the fraction of space-time occupied by instantons) of these ensembles is $f=0.05$ and 0.60, respectively, to be compared with $f=0.06$ in the original instanton liquid model. The variational method was extended to light quarks in [43,36,26,24]. We will study this problem in detail in the next section.

If correlations among instantons are important, the variational method is not expected to provide an accurate estimate for the partition function and other observables. Since the main source of correlations in the instanton liquid are dynamical quarks, this issue is particularly important for real QCD with two light and one intermediate mass flavors. Also, as argued in the Introduction, we expect chiral symmetry to be restored because of the formation of instanton–anti-instanton molecules. This feature is certainly not captured by the variational model (at least not in its simplest form), and we will therefore study the full partition function numerically using the method introduced in this section.

## IV. THE INSTANTON ENSEMBLE AT ZERO TEMPERATURE

In this section we want to present numerical results obtained from simulations of the instanton liquid at zero temperature. While the streamline *Ansatz*, in principle, provides the ''best'' classical interaction, its derivation relies heavily on conformal symmetry and we do not know how to extend it to finite temperature. In Sec. VI, we will therefore give a brief discussion of the ratio *Ansatz* ensemble at zero temperature.

A general problem with calculations in the interacting instanton model is the treatment of very close instanton–anti-instanton pairs. On the one hand, these configurations do not contribute significantly to physical observables, such as the quark condensate, hadronic masses, or the topological susceptibility. Very close instanton–anti-instanton pairs with an attractive relative orientation correspond to perturbative fluctuations and should not be taken into account as a nonperturbative effect. On the other hand, the partition function of the instanton liquid introduced in the last section treats even very close pairs as two independent pseudoparticles. Especially in the streamline *Ansatz*, which provides very little short range repulsion, this means that close pairs can contribute significantly to the free energy of the system. Ideally, one would need a consistent determination of the space of collective variables for very close pairs and a subtraction procedure for purely perturbative fluctuations. Unfortunately, such a method is not available at present. There is an interesting suggestion to define the instanton interaction (via the optical theorem) by the cross section for isotropic multigluon production [44]. In this case, the existence of a short range

TABLE I. Parameters of the pure gauge instanton ensemble in the streamline *Ansatz* for various values of the core parameter $A$. The density and average instanton size are given in units of $\Lambda_{\rm QCD}$ and fm. The dimensionless scale parameter $f$ is introduced in the text.

| $A$ | $N/V[\Lambda_{\rm QCD}^4]$ | $\rho[\Lambda_{\rm QCD}^{-1}]$ | $f$ | $\Lambda_{\rm QCD}$ [MeV] | $N/V$ [fm$^{-4}$] | $\rho$ [fm] |
|---|---|---|---|---|---|---|
| 24 | 0.97 | 0.60 | 0.62 | 202 | 1.00 | 0.59 |
| 64 | 0..41 | 0.58 | 0.16 | 250 | 1.00 | 0.45 |
| 128 | 0.30 | 0.58 | 0.12 | 270 | 1.00 | 0.43 |
| 256 | 0.18 | 0.55 | 0.08 | 307 | 1.00 | 0.36 |

core in the instanton interaction is related to the question whether the multigluon production cross section at high energy can reach the unitarity bound. If, as it has been suggested in [45] and other works on the subject, the cross section only grows until it reaches a square root suppression and then turns, the instanton–anti-instanton interaction would decrease until it reaches a minimum at which $S_{\rm int}=-S_0$, and then show a short distance repulsive core.

In practice, we have decided to deal with the problem of very close pairs in the streamline *Ansatz* by introducing a purely phenomenological short range repulsive core

$$S_{\rm core}=\beta_1(\overline{\rho})\frac{A}{\lambda^4}|u|^2,$$

$$\lambda=\frac{R^2+\rho_I^2+\rho_A^2}{2\rho_I\rho_A}+\left(\frac{(R^2+\rho_I^2+\rho_A^2)^2}{4\rho_I^2\rho_A^2}-1\right)^{1/2} \qquad (21)$$

in both the $II$ and $IA$ interactions. The orientational factor $\propto|u|^2$ ensures that the repulsion is reduced for instantons in different SU(2) embeddings. The interaction is repulsive, independent of the relative orientation $\cos\theta$. $\lambda$ is the conformal parameter that determines the functional form of the streamline interaction [35] and $A$ controls the strength of the core. This parameter governs the dimensionless diluteness $f=0.5\pi^2\rho^4(N/V)$ of the instanton ensemble.

The second parameter of the instanton liquid is the scale $\Lambda_{\rm QCD}$ in the partition function, which fixes the physical units. Although $\Lambda_{\rm QCD}$ is known, in principle, from perturbative QCD, the accuracy of these determinations is not very high and quantities such as the instanton density $(N/V)\sim\Lambda_{\rm QCD}^4$ are very sensitive to the precise numerical value of the scale parameter. As in lattice calculations, one may therefore fix the scale using the value of some observable, for example a hadronic mass, as the basic unit. Which quantity to hold fixed while comparing different theories, e.g., quenched and unquenched calculations, is pure convention. We have decided to proceed in a very simple way and fix our units such that $N/V=1$ fm$^{-4}$ in all cases. This means that in this work 1 fm is, by definition, the average distance between instantons (at $T=0$). The corresponding instanton density agrees well with the lattice measurements mentioned above and corresponds to the canonical value of the gluon condensate, $(\alpha_s/\pi G^2)=(350\ {\rm MeV})^4$.

We have studied the instanton ensemble for various values of the core parameter $A$. The results are summarized in Table I. The minimal value of $A$ needed in order to stabilize the ensemble is $A\simeq16$. Increasing the core, one obviously makes the ensemble more dilute. However, as the interaction becomes more repulsive, the density in units of the scale parameter drops and one has to increase the value of $\Lambda_{\rm QCD}$ in order to keep the physical density fixed. In practice, we have chosen $A=128$, so that $\Lambda_{\rm QCD}$ remains below 300 MeV, which is roughly the upper limit of the experimental uncertainty. As a consequence, the ensemble is not as dilute as suggested by phenomenology ($n=1$ fm$^{-4}$ and $\rho=0.33$ fm), but the diluteness is comparable to the lattice result $n=(1.4$–$1.6)$ fm$^{-4}$ and $\rho=0.35$ fm [17]. Two more important parameters of the ensemble are the average instanton action $S=(8\pi^2)/g^2$ and the average interaction $S_{\rm int}/N$ per instanton. For $A=128$, we find $S\simeq6.4$ and $S_{\rm int}/N\simeq1.0$, showing that the system is still semiclassical and that interactions among instantons are important, but not dominant.

Detailed results of our simulations for $A=128$ are shown in Figs. 2–5. The partition function at each instanton density was determined by generating 5000 configurations with 32 instantons at 10 different coupling constants $\alpha$. The variational *Ansatz* (16) for the partition function was determined from 600 initial sweeps with the full interaction ($\alpha=1$). The integral (17) was determined by gradually lowering the coupling to $\alpha=0$ and then raising it back to $\alpha=1$ (hysteresis method). The difference in the results between the up and down sweeps provides an estimate of the error in the integral due to incomplete equilibration. The average between the up and down sweeps usually provides a good estimate for the correct result, even if equilibration is slow (as will be the case close to the phase transition).

Figure 2(a) shows the free energy vs the instanton density (in units of $\Lambda^4$) for the pure gauge theory (without fermions). At low density the free energy is roughly proportional to the density, but at larger densities repulsive interactions become important, leading to a well-defined minimum. We also show the average action per instanton as a function of the density. The average action controls the probability $\exp(-S)$ to find an instanton, but has no minimum in the range of densities studied. This shows that the minimum in the free energy is a compromise between maximum entropy and minimum action.

Fixing the units such that $N/V=1$ fm$^{-4}$, we have $\Lambda=270$ MeV and the vacuum energy density generated by instantons is $\epsilon=-526$ MeV/fm$^3$. This important quantity is related to the gluon condensate by the trace anomaly

$$\epsilon=-\frac{b}{128\pi^2}\langle g^2G^2\rangle, \qquad (22)$$

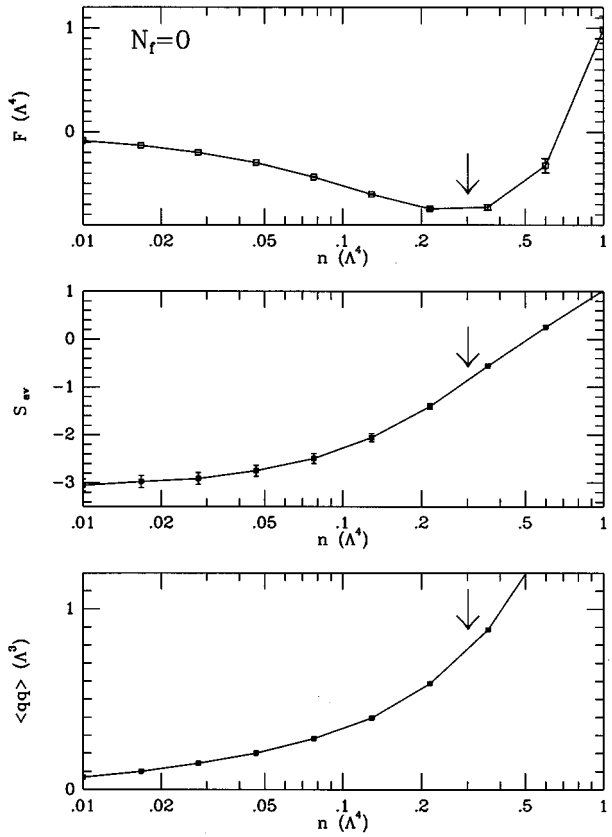


FIG. 2. Free energy, average instanton action, and quark condensate as a function of the instanton density in the pure gauge theory. All quantities are given in units of the scale parameter $\Lambda_{\rm QCD}$.

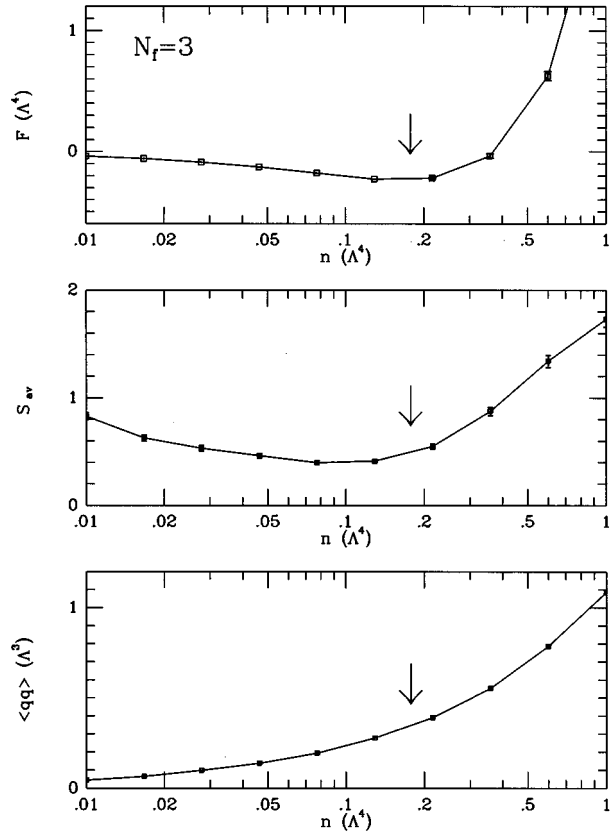


FIG. 3. Free energy, average instanton action, and quark condensate as a function of the instanton density in the theory with two light and one intermediate mass flavors. All quantities are given in units of the scale parameter $\Lambda_{\rm QCD}$.

where $b=\frac{11}{3}N_c$ in the pure gauge case. For a sufficiently dilute system of instantons,[1] the gluon condensate is simply proportional to the instanton density, $\epsilon=-b/4(N/V)=-565$ MeV/fm$^3$. The good agreement of this number with the energy density determined above shows that our calculation is consistent with the trace anomaly. This is also true for the variational method [7], as indeed one would expect for any calculation that does not introduce any dimensionful scale except for $\Lambda$. Also note that not only the depth of the free energy, but also its curvature (the instanton compressibility), is fixed from a general theorem. From standard thermodynamical relations, the compressibility is related to the mean square fluctuation of the particle number. This quantity is determined by a low energy theorem derived by Novikov *et al.* [46]:

$$\int d^4x\langle g^2G^2(x)g^2G^2(0)\rangle=\frac{128\pi^2}{b}\langle g^2G^2\rangle. \qquad (23)$$

Similar to the trace anomaly (22), this relation follows from the renormalization properties of QCD. Saturating (23) with a dilute system of instantons, one has $\langle(\Delta N)^2\rangle=4/bN$, where $\Delta N$ is the mean fluctuation of the number of instantons in a volume $V$. For the compressibility of the instanton liquid, this implies

$$\frac{\partial^2 F}{\partial(N/V)^2}=\frac{b}{4}\left(\frac{N}{V}\right)^{-1}. \qquad (24)$$

We have determined the compressibility from our data and find it to be $3.2(N/V)^{-1}$, compared with $2.75(N/V)^{-1}$ from Eq. (24). We have also studied density fluctuations in the interacting instanton liquid [21,13] and have found good agreement with the low energy theorem (see also [7,47]).

Next, we study the effects of light quarks on the instanton ensemble. A problem that is well known in lattice simulations is the fact that finite volume effects are more severe in the presence of light fermions. These ''mesoscopic'' effects become important if the mass of the Goldstone bosons $m_\pi\sim\sqrt{m\Lambda}$ is comparable to the inverse box size $1/L$. In order to avoid these problems, one is often forced to work with light quark masses that are larger than their physical values. The calculations reported below were performed with light quark masses $m_u=m_d=0.1\Lambda$, while the strange quark mass is $m_s=0.7\Lambda$. If one makes the quark mass smaller while keeping the volume fixed, then chiral symmetry breaking will eventually disappear.

The free energy as a function of the instanton density in full QCD is shown in Fig. 3(a). We find that the free energy looks very similar to the pure gauge case, but the minimum is shifted to a smaller density $N/V=0.174\Lambda^4$. With our convention $N/V=1$ fm$^{-4}$ as above, the scale is given by $\Lambda=310$ MeV. This gives the instanton-induced vacuum en-

[1]As mentioned above, the average interaction is only a 15% correction to the single instanton action.

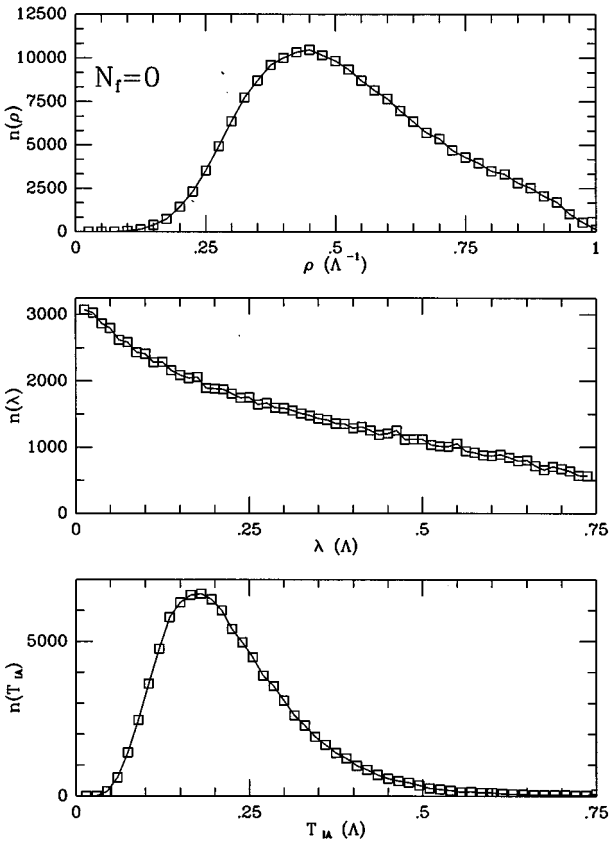


FIG. 4. Distribution of instanton sizes, eigenvalue spectrum of the Dirac operator, and distribution of fermionic overlap matrix elements in pure gauge theory. $\rho,\lambda$ and $T_{IA}$ are given in units of the scale parameter. The distribution functions have arbitrary units.

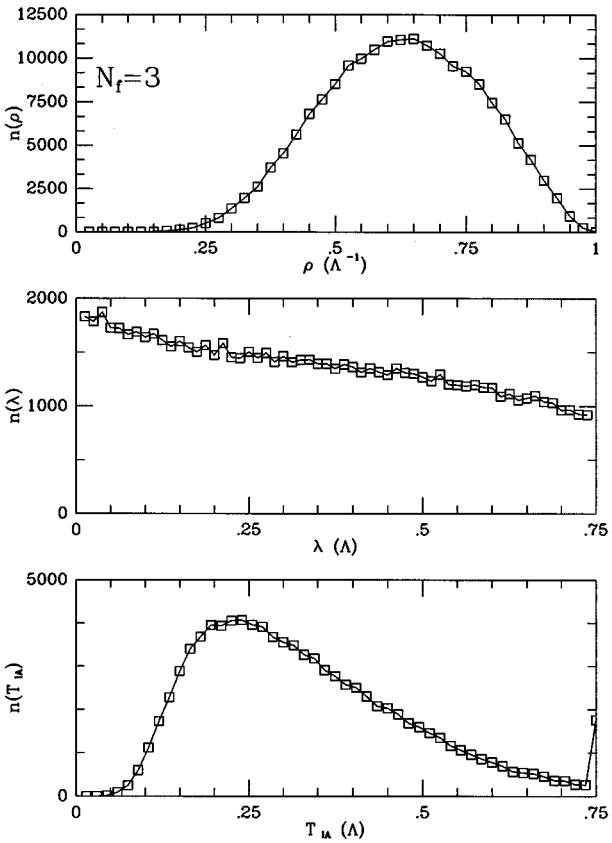


FIG. 5. Distribution of instanton sizes, eigenvalue spectrum of the Dirac operator, and distribution of fermionic overlap matrix elements in full QCD.

ergy $\epsilon=-280$ MeV/fm$^3$, which is smaller as compared to that in the pure gauge case. In the presence of quarks, the trace anomaly gives[2]

$$\epsilon=-\frac{b}{128\pi^2}\langle g^2G^2\rangle+\sum_f\frac{1}{4}m_f\langle\overline{q_f}q_f\rangle. \tag{25}$$

The main difference as compared to the pure gauge case is that the Gell-Mann–Low coefficient is changed from $b=11$ to $b=9$ (for $N_f=3$). Estimating the gluon condensate from the instanton density as above, we get $\epsilon=-488$ MeV/fm$^3$. This number does not agree very well with the value extracted from the free energy. One possible reason is that interactions are more important in the full ensemble so that the gluon condensate is not proportional to the instanton density. Another problem might be connected with the value of the quark mass. As mentioned above, if one enters the regime of mesoscopic QCD, one may encounter additional scale breaking not described by the trace anomaly. We indeed find that the scale anomaly can be saturated with the instanton density for larger quark masses.

At the minimum of the free energy, we can also determine the quark condensate [see Fig. 3(c)]. In full QCD, we find $\langle\overline{qq}\rangle=-(216\text{ MeV})^3$, which is in good agreement with the phenomenological value. This value can also be compared to the quark condensate in quenched QCD [calculated in the pure gauge configurations, see Fig. 2(c)] $\langle\overline{qq}\rangle=-(251\text{ MeV})^3$, showing that light quarks suppress the quark condensate.

Additional information about the ensemble is provided by the distribution of the instanton sizes, Dirac eigenvalues, and fermionic overlap matrix elements. In Figs. 4 and 5, we present these distributions for the two cases discussed above. The instanton size distribution shows the perturbative $\rho^{b-5}$ behavior at small sizes, has a maximum (at $\rho=0.50\Lambda^{-1}$ in quenched and $\rho=0.65\Lambda^{-1}$ in full QCD) and falls off for larger sizes. The average sizes are $\rho=0.43$ fm in quenched and $\rho=0.42$ fm in full QCD. The diluteness parameter in the full ensemble is $f=0.14$, compared with $f=0.17$ in the quenched calculation.

The distribution of eigenvalues of the Dirac operator, $i\hat{D}\psi_\lambda=\lambda\psi_\lambda$, contains a lot of useful information about the spectrum of the theory. We will discuss some of these questions in more detail below. Here, we only mention that the Banks-Casher relation, $\langle\overline{qq}\rangle=-\rho(\lambda=0)/\pi$, connects the density of eigenvalues of the Dirac operator near zero with the chiral condensate. From Figs. 4(b) and 5(b), one clearly

[2]Despite the factor 1/4 in front of the quark condensate contribution, this relation is consistent with the general result $\langle\overline{q_f}q_f\rangle=\partial/\partial m_f\ln Z$. The remaining mass dependence of the vacuum energy density comes from the gluon condensate, $\partial/\partial m_f\langle g^2G^2\rangle=-96\pi^2/b\langle\overline{q_f}q_f\rangle$, which is valid for light quarks.

observes that the instanton liquid leads to a nonvanishing density of eigenvalues near $\lambda = 0$. The results also show that the presence of light quarks suppresses the number of small eigenvalues. While the spectrum is peaked towards small eigenvalues in the purge gauge case, it is essentially flat in full QCD. This is consistent with the prediction from chiral perturbation theory [48]:

$$\rho(\lambda) = -\pi\langle\overline{qq}\rangle + \frac{\langle\overline{qq}\rangle^2}{32\pi^2 f_\pi^4}\frac{N_f^2-4}{N_f}|\lambda| + \cdots, \qquad (26)$$

which is valid for $N_f \geq 2$ (no definite results are known for $N_f = 0,1$, see, for example, [49]). The second term is zero[3] for $N_f = 2$ and leads to a singular behavior for $N_f > 2$. No such dip is seen in our spectrum, showing that the result is closer to the $N_f = 2$ case. More detailed studies of the spectrum of the Dirac operator in the instanton liquid for various number of colors and flavors were reported in [50].

In Figs. 3(c) and 4(c), we also show the distribution of the largest fermionic overlap matrix elements $T_{IA}$ for each instanton. For each instanton, we select the anti-instanton it has the largest overlap with and plot the resulting distribution of matrix elements. This distribution is a measure of the strength of correlations among the instantons. For a completely random system at the same density as the simulated quenched and fully interacting ensembles, the average overlap would be $T_{IA} = 0.22\Lambda$ and $T_{IA} = 0.21\Lambda$, respectively. Instead, the measured distributions have an average $0.23\Lambda$ and $0.33\Lambda$, showing that correlations are not very important in the quenched ensemble, but play only some role in the full ensemble. A more physical measure of the importance of correlations among instantons is given by the dependence of hadronic correlation functions on different ensembles. We will study this question in some detail in a forthcoming publication.

## V. THE PHASE DIAGRAM OF THE INSTANTON LIQUID

After fixing the overall scale at zero temperature, it is now straightforward to extend our calculation to finite temperature. In an Euclidean field theory, finite temperature only enters through the boundary conditions obeyed by the fields. The gauge fields have to be periodic in the Euclidean time direction with the period given by the inverse temperature, while fermions are subject to antiperiodic boundary conditions. The corresponding periodic instanton and fermion zero-mode profiles can be constructed using 't Hooft's multi-instanton solution [51]. These profiles may then be used to study the instanton interaction and fermionic overlap matrix elements. For the ratio *Ansatz*, such a study was performed in [52]. A parametrization of this interaction is given in Appendices C and D.

The most important qualitative feature of the instanton interaction at finite temperature is the form of the fermionic overlap matrix elements. The determinant for one instanton–anti-instanton pair separated by $\tau$ in Euclidean time and $r$ in the spatial direction is roughly proportional to

$$\det(i\hat{D}) \sim \left|\frac{\sin(\pi T\tau)}{\cosh(\pi T r)}\right|^{2N_f}. \qquad (27)$$

The form of this interaction is a simple consequence of the periodicity in the time direction and the fact that fermion propagators are screened in the spatial direction by the lowest Matsubara frequency $\pi T$. The interaction clearly favors instanton–anti-instanton pairs (molecules) that are aligned along the time direction with a separation $\tau = 1/(2T)$. Ilgenfritz and Shuryak [31] proposed that this feature of the interaction leads to a phase transition in the instanton liquid. In this phase transition, the system goes from a random liquid to an ordered phase of instanton–anti-instanton molecules. The transition was studied in a schematic model in [31,32]. In the present work we want to test whether a consistent treatment of the full partition function of the instanton liquid does indeed lead to the expected phase transition and performs a quantitative study of bulk properties of the system near the transition.

Before we consider the QCD case (with two light and one intermediate mass flavors) in detail, it is instructive to study the phase diagram of the instanton liquid for a wider range of theories. In order to cover many different parameters, we have restricted ourselves to an exploratory study, in which we do not minimize the free energy of the system, but consider the instanton ensemble at fixed density. Using the same convention employed in the last section, this density was chosen to be 1 fm$^{-4}$. In our experience, if the system undergoes a phase transition, it will do so even if the density is not determined self-consistently, although at a somewhat different temperature. Nevertheless, before this point is checked in detail, the results presented in this section should be considered qualitative.

We first consider the situation for only one quark flavor. In this case, the only chiral symmetry is the anomalous axial $U_A(1)$, so there are no Goldstone pions, but only a flavor singlet (the analogue of the $\eta'$). Therefore, one would not expect a chiral restoration phase transition. On the other hand, a (first-order) transition may exist even without a symmetry, and in principle, the general argument concerning the formation of *IA* molecules also applies to the case $N_f = 1$. Clearly, fermion-induced correlations become stronger as the number of flavors increases. Whether they are strong enough for $N_f = 1$ to induce a phase transition has to be determined from the partition function.

We have studied the $N_f = 1$ system at an instanton density $N/V = 1$ fm$^{-4}$ for temperatures up $T \simeq 300$ MeV. We have observed no phase transition in this range, the condensate $\langle\overline{qq}\rangle$ decreases smoothly, and is nonzero even at the highest temperature studied. Of course, even in pure SU(3) Yang-Mills theory (without fermions), lattice simulations find a strong first-order deconfinement phase transition at a temperature[4] $T \simeq 250$ MeV. The interacting instanton model,

[3]This result is connected with the fact that for $N_f > 2$, there is a Goldstone boson cut appearing in the scalar isovector ($\delta$ meson) correlator, while there is no $\delta \to \pi\pi$ decay allowed for two flavors.

[4]Again, we note that specifying the temperature in physical units in a quenched calculation requires a procedure to set the scale. In practice this is done, for example, by keeping the (quenched) $\rho$ meson mass fixed.

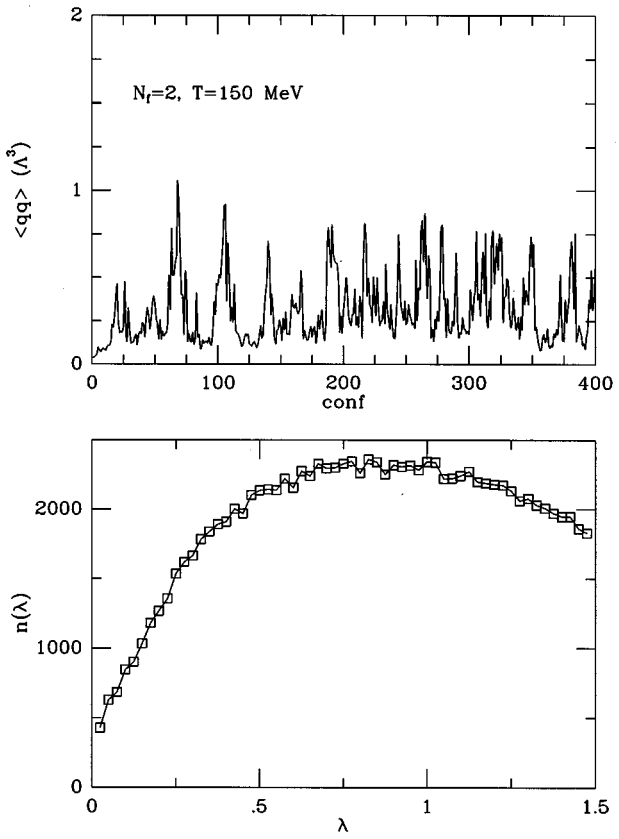


FIG. 6. Trajectory of the quark condensate (in units of $\mathrm{fm}^{-3}$) for $N_f=2$ in the critical region, $T=150$ MeV. We also show the corresponding spectrum of Dirac eigenvalues $\lambda$ [$\mathrm{fm}^{-1}$]. The normalization of the eigenvalue distribution is arbitrary.

however, does not give confinement, so, naturally, there is no deconfinement transition.

The case of two light flavors, $N_f=2$, is quite special. According to standard universality arguments [53,54], the chiral phase transition is expected to be of second order, with the same critical behavior as the O(4) Heisenberg magnet in $d=3$ dimensions.[5] We have simulated $N_f=2$ ensembles for various temperatures and values of the quark masses. For sufficiently small quark masses $m<0.15\Lambda$, we find large fluctuations in the condensate at $T\simeq 150$ MeV. To illustrate this fact, we show a typical time history of the quark condensate in Fig. 6(a). Every configuration corresponds to one complete sweep through the instanton ensemble, with one Metropolis hit performed on every collective variable. It is clear that the transition is either second order or first order with a very small barrier between the two phases. In order to distinguish these two possibilities, one would have to perform a finite-size scaling analysis, which goes beyond the scope of this paper. We will see later that for more flavors, there is a barrier between the two phases. In Fig. 6(b) we show the Dirac spectrum for $T=150$ MeV and $m=5$ MeV. The eigenvalue density extrapolates to zero at $\lambda=0$, but the slope is very steep and there are no signs of a gap in the spectrum.

We will treat the three-flavor case in detail in the next section, and now proceed to the case of several flavors of light quarks. Let us first mention several theoretical arguments suggesting qualitative changes in the vacuum structure as $N_f$ increases beyond some critical value $N_f^{\mathrm{crit}}$.

A simple phenomenological observation is the fact that for $N_f>12$, the number of ''pions'' $N_\pi=N_f^2-1$ exceeds the number of quarks and antiquarks $N_q=4N_cN_f$. This prevents the usual matching of the pion gas at low temperature to the high-$T$ quark-gluon plasma phase with a positive bag constant. It seems plausible that something should happen before this point is reached, so $N_f^{\mathrm{crit}}<12$.

As noticed by a number of authors (see, e.g., [58]), the second coefficient $b'$ of the beta function changes sign for smaller $N_f$ than the first one $b$ does. In this window, one has the possibility of asymptotic freedom coexisting with an infrared fixed point.

It was recognized in [59,9] that for large $N_f$, the instanton liquid is dominated by instanton molecules, and that their density is UV divergent (at small radii) if $2b-5<0$, corresponding to $N_f>12$ (this estimate is slightly modified if interactions are taken into account [39]). This divergence, however, is a short distance effect and should not affect physical observables.

Lattice simulations of QCD for large $N_f$ were performed by Iwasaki *et al.* [60]. They found that for $N_c=2$, the critical number of flavors for which chiral symmetry is restored is $N_f^{\mathrm{crit}}=3$, while for $N_c=3$, it is $N_f^{\mathrm{crit}}=7$. A strange ''bulk transition'' was also observed by the Columbia group for $N_f=8$ [61].

Finally, significant progress has been made in understanding $N=1$ supersymmetric generalizations of QCD [62]. One result that is of particular interest in the present context is the exact determination of the critical number of flavors $N_f^{\mathrm{crit}}=N_c+1$, where chiral symmetry is broken for $N_f\leqslant N_f^{\mathrm{crit}}$, but not for $N_f>N_f^{\mathrm{crit}}$.

We should stress that in QCD, anomaly matching implies (for $N_f>2$) that if chiral symmetry is restored in the ground state, the theory is also not confining. This connection, of course, cannot be studied in the instanton model. Having said this, let us now report our results concerning the vacuum structure of the instanton liquid for many flavors. A useful tool to analyze the structure of chiral symmetry breaking that was suggested by the Columbia group [63] is the ''valence quark mass'' dependence of the quark condensate, defined by

$$\langle\overline{q}q(m_v)\rangle=-\int d\lambda\rho(\lambda,m)\frac{2m_v}{\lambda^2+m_v^2}. \tag{28}$$

Here, $\rho(\lambda,m)$ is the eigenvalue density of the Dirac operator calculated from configurations generated with dynamical mass $m$. The quark condensate in the chiral limit is defined by going to the thermodynamic limit and then taking $m=m_v\to 0$. In a finite system, however, chiral symmetry is never broken at nonzero quark mass and one has to perform

[5]Recently, Kocic and Kogut [55] have challenged these arguments and suggested that the transition is indeed second order, but with mean field exponents. Lattice results (see [56] and the review [57]) seem to verify that the transition is second order, but are not yet sufficiently accurate to resolve the issue about the critical exponents.

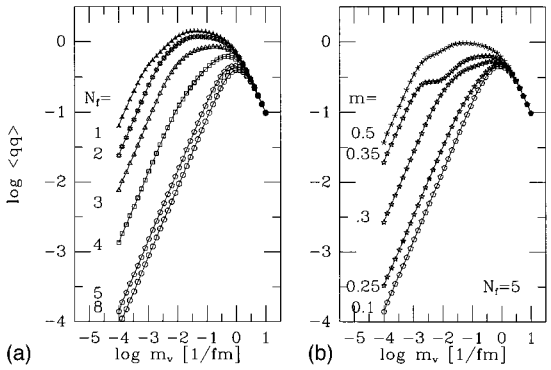


FIG. 7. (a) Double logarithmic plot of the quark condensate (in units of $\mathrm{fm}^{-3}$) vs the valence quark mass $m_v$ for different number of light flavors (with dynamical mass $m=20$ MeV). (b) shows the same plot for $N_f=5$ and different quark masses $m$. The logarithm is to base 10.

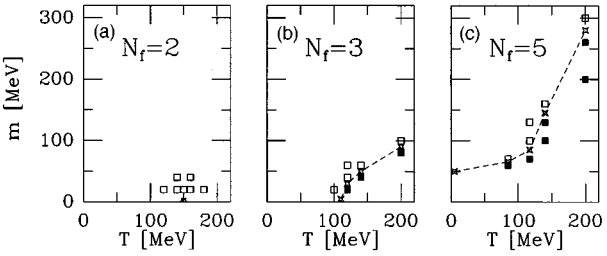


FIG. 8. Schematic phase diagram of the instanton liquid for different numbers of quark flavors, $N_f=2$, 3, and 5. We show the phase of chiral symmetry breaking in the temperature-quark mass planes. (a) For $N_f=2$, open squares indicate points where we found large fluctuations of the chiral condensate, the cross indicates the approximate location of the singularity. In the two other figures (b) and (c) the open squares correspond to points where we find a plateau in the valence mass dependence of the chiral condensate, while solid squares correspond to points where such a plateau is absent. The crosses and the dashed lines connecting them show the approximate location of the discontinuity line.

a detailed scaling analysis. This analysis amounts to performing many simulations at various values of the dynamical mass, which is a very time consuming procedure. Instead, one might get a good indication of the full behavior by studying the valence mass dependence of the condensate. At very small $m_v$, the condensate is proportional to $m_v$, which means that one is sensitive to induced rather than spontaneous chiral symmetry breaking. At very large mass $m_v$, the condensate is proportional to $m_v^{-1}$. Both of these limits are of course unphysical, and spontaneous symmetry breaking in the continuum limit is indicated by the appearance of a plateau at intermediate values of the valence mass where $\langle\overline{qq}\rangle$ depends only weakly on $m_v$.

In Fig. 7 we show a number of calculations of the valence mass dependence of the condensate. The results in Fig. 7(a) were obtained for 64 instantons in a cubic box $V=(2.828\ \mathrm{fm})^4$ (corresponding to a density $N/V=1\ \mathrm{fm}^{-4}$ and a fairly low temperature, $T=71$ MeV), with the dynamical quark mass $m=20$ MeV and different number of flavors $N_f=1,\ldots,8$. Regions where the condensate depends only weakly on $m_v$ are clearly seen for $N_f=1,2,3$. These plateaus are clearly absent for $N_f=5$ or larger: we therefore conclude that the instanton liquid model has a chirally symmetric ground state in these cases. A more detailed study of the configurations shows that all instantons are bound into molecules. The borderline case appears to be $N_f=4$: if a condensate is present, it is significantly smaller than in QCD and due to a relatively small random component of the vacuum.

We have also performed simulations for two colors, and obtained a similar picture, but with the critical number of flavors smaller by 1. For $N_c=2$ no clear signal of chiral symmetry breaking was observed for $N_f\geqslant 3$. This suggests the empirical relation $N_f^{\mathrm{crit}}=N_c+C$ with $1<C<2$, an amusing coincidence with Seiberg's results for $N=1$ supersymmetric QCD [62].

The next question we would like to address is the dependence of these results on the dynamical quark mass $m$. Increasing the dynamical mass, one decreases the influence of quark determinant. A large quark mass works against the correlations induced by a large number of flavors. This means that for a sufficiently large quark mass, one can find ''spontaneous'' symmetry breaking even if there is no symmetry breaking in the chiral limit. This is demonstrated in Fig. 7(b), where we show a series of calculations for $N_f=5$, with the dynamical quark mass $m$ ranging from 20 to 100 MeV. In this case a plateau in the valence mass dependence of the condensate reappears at rather small critical quark mass of about 35 MeV.

Repeating these studies for different numbers of flavors and varying the mass and temperature, one can map the phase diagram of the instanton liquid in the $T-m$ (temperature-mass) plane. In Fig. 8 we have summarized our results for $N_f=2$, 3, and 5. Those cases in which we found a signal for chiral symmetry breakdown are marked by the open squares, and those corresponding to the restored phase by solid squares. The (approximate) location of the discontinuity line between the two phases is marked by the stars connected by dashed lines. For two flavors we do not find such a line of discontinuities. We have performed a number of runs in the vicinity of the phase transition, all showing large fluctuations of the condensate. For larger $N_f$ we clearly see a transition line with a discontinuity of the condensate. When the number of flavors increases, one end of this line moves to the left (the critical temperature $T_c$ decreases with $N_f$), crossing zero somewhere around $N_f=4$, but before $N_f=5$. In these cases, the ground state exhibits spontaneous symmetry breaking only if the quark mass exceeds some critical value. For technical reasons, we have not tried to follow the discontinuity lines much beyond $T>200$ MeV. In this regime, the condensate becomes more and more dominated by few extremely small eigenvalues, so that numerical accuracy starts to become a concern. In addition to that, one does not expect to be able to describe possible transitions at very large temperature in the instanton model, since these will presumably be dominated by the pure gauge deconfinement transition.

## VI. THE INSTANTON ENSEMBLE IN QCD AT FINITE TEMPERATURE

In this section we want to discuss in detail the physically relevant case of two light and one intermediate mass flavors.

In particular, we will perform self-consistent simulations where the correct instanton density is determined from minimizing the free energy. The instanton interaction and fermionic matrix elements that enter these calculations have already been discussed in the last section. The semiclassical calculation that leads to the instanton distribution (3) has also been generalized to finite temperature [25], giving

$$d(\rho,T)=d(\rho,T=0)\exp[-\tfrac{1}{3}(2N_c+N_f)(\pi\rho T)^2-B(z)],$$

$$B(z)=\left(1+\frac{N_c}{6}-\frac{N_f}{6}\right)\left[-\ln\left(1+\frac{z^2}{3}\right)+\frac{0.15}{(1+0.15z^{-3/2})^8}\right], \tag{29}$$

with $z=\pi\rho T$. This correction factor leads to an exponential suppression of large instantons at high temperature. Its origin is mainly the scattering of thermal gluons on the instanton. This phenomenon is related to the Debye mass, which, in fact, has the same dependence on $N_c$ and $N_f$. The applicability of (29) is controlled by two separate conditions, $\rho\ll\Lambda^{-1}$ to ensure the semiclassical treatment, and $T\gg\Lambda$ to justify a perturbative treatment of the heat bath. It was therefore argued in [28] that one should not use the perturbative suppression factor (29) at temperatures below the phase transition. This suggestion was indeed verified by lattice simulations for pure gauge theory [29], which found a very weak temperature dependence of the instanton density below $T_c$, and an exponential suppression of instantons consistent with (29) above $T_c$. In practice, we have determined the phase transition temperature without the suppression factor (29). The final simulations were then performed with an additional temperature-dependent factor $[1-\tanh(T-T_c/\Delta T)]/2$ inserted in the exponential appearing in Eq. (29). From our simulations, we have determined $T_c\simeq 0.75\Lambda$. We have taken $\Delta T\simeq 0.2\Lambda$. This number characterizes the temperature range over which the Debye mass reaches its perturbative value and is roughly consistent with the result of lattice simulations [64]. In our simulations, the value of $\Delta T$ determines how fast the instanton density drops above $T_c$. On the other hand, we have checked that the temperature dependence of the quark condensate is almost independent of this parameter.

With all the ingredients of the partition function fixed, we can proceed to our simulations. The free energy is determined as described in Secs. III and IV. There is no difficulty in principle associated with applying the adiabatic switching method at finite temperature. In practice, however, some care is required since, in case the system undergoes a phase transition, the ensemble at the full coupling $\alpha=1$ is in a different phase as compared to the random distribution at $\alpha=0$. This implies that the transition will occur at some value of $\alpha$ during the adiabatic switching. The hysteresis method described in Sec. IV is particularly well suited to handle a situation such as this. Physically, this simply means that the variational *Ansatz* (16), while it is still used as a reference distribution, ceases to be a good approximation to the fully interacting instanton distribution. In the whole range of temperatures studied, we find that the behavior of the free energy as a function of the instanton density looks qualitatively similar to the zero temperature result shown in Figs. 2 and 3. In particular, the free energy is negative at small density and has one fairly well-defined minimum. This means that the phase transition is either smooth or a first-order transition with a small jump in the instanton density, which we cannot resolve because of finite-size effects.

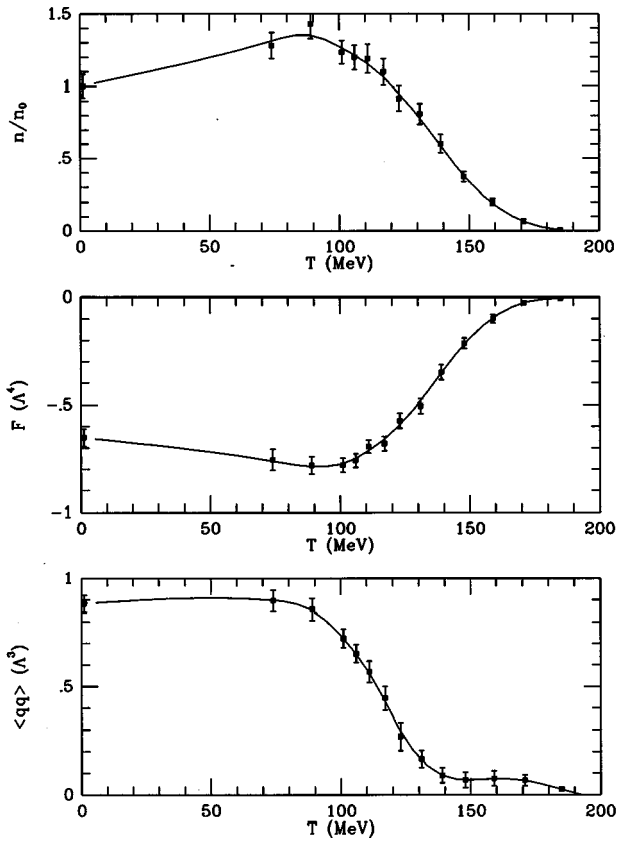


FIG. 9. Instanton density, free energy, and quark condensate as a function of the temperature in full QCD with two light and one intermediate mass flavors.

The resulting instanton density, free energy, and quark condensate are shown in Fig. 9. In the ratio *Ansatz*, the instanton density at zero temperature is given by $N/V=0.69\Lambda^4$. Taking the density to be 1 fm$^{-4}$ at $T=0$, fixes the scale parameter $\Lambda=222$ MeV and determines the absolute units. The temperature dependence of the instanton density is shown in Fig. 9(a). It shows a slight increase at small temperatures,[6] starts to drop around 115 MeV, and becomes very small for $T>175$ MeV. The free energy closely follows the behavior of the instanton density. This means that the instanton-induced pressure first increases slightly, but then drops and eventually vanishes at high temperature. This behavior is expected for a system of instantons, but in a complete theory with perturbative effects included, the pressure should always increase as a function of the temperature. In QCD, the pressure at high temperature is of course provided by the black body contributions from quarks and gluons. We will come back to this issue at the end of the section.

The temperature dependence of the quark condensate is

[6]The zero temperature point corresponds to a simulation with zero temperature matrix elements in a periodic box $V=(2.828\Lambda^{-1})^4$, so it is not a true zero temperature calculation.

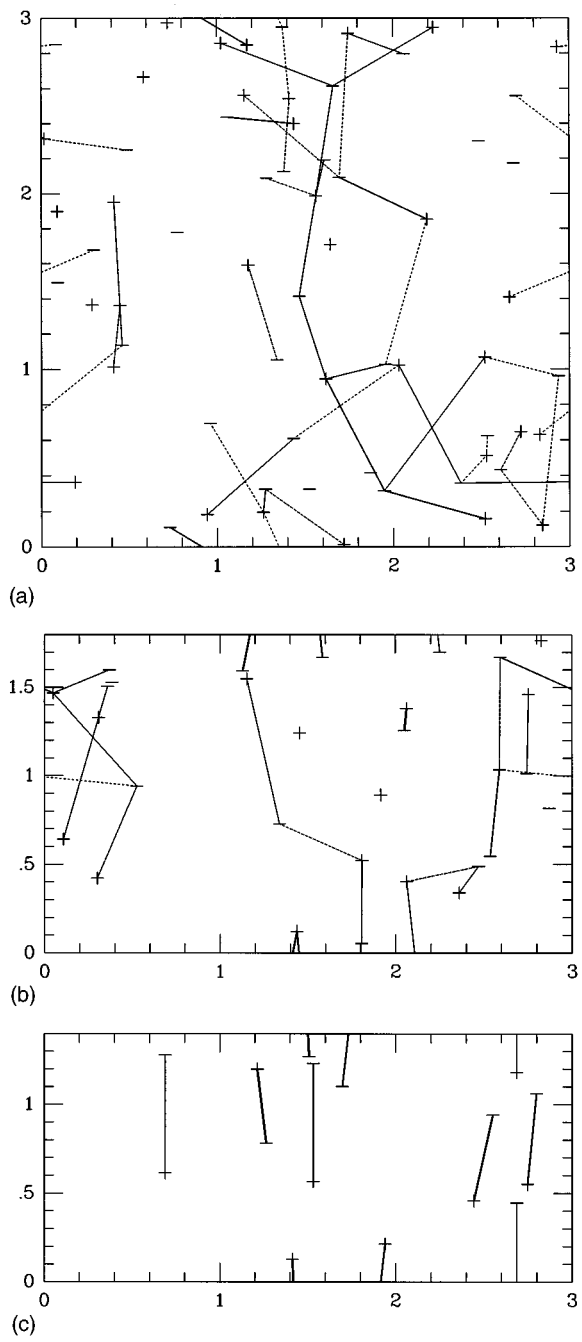


FIG. 10. Typical instanton ensembles for $T=75$, 123, and 158 MeV. The plots show projections of a four-dimensional $(3\Lambda^{-1})^3\times T^{-1}$ box into the 3-4 ($z$ axis-imaginary temperature) plane. Instantons and anti-instanton positions are indicated by + and − symbols, respectively. Dashed, solid, and thick solid lines correspond to fermionic overlap matrix elements $T_{IA}>0.40,0.56,0.64\ \Lambda$, respectively.

shown in Fig. 9(c). At temperatures below $T=100$ MeV, it is practically temperature independent. It then starts to drop fast and becomes very small around the critical temperature $T\simeq 140$ MeV. Note that at this point the instanton density is $N/V=0.6\ \mathrm{fm}^{-4}$, slightly more than half the zero temperature value. This means that the phase transition is indeed caused by a transition within the instanton liquid, not by the disappearance of instantons. This is illustrated by Fig. 10, which shows snapshots of the instanton liquid at temperatures $T=74$, 123, 158 MeV below, near, and above the chiral phase transition. The figures are projections of a four-dimensional cube $V=(3.00\Lambda^{-1})^3\cdot 1/T$ into the 3-4 plane. The positions of instantons and anti-instantons are denoted by + and − symbols, respectively. The lines connecting them indicate the strength of the fermionic overlap matrix elements. Below the phase transition, there is no clear pattern. Instantons are unpaired, part of molecules, or larger clusters. As the phase transition progresses, one clearly observes the formation of polarized instanton–anti-instanton molecules.

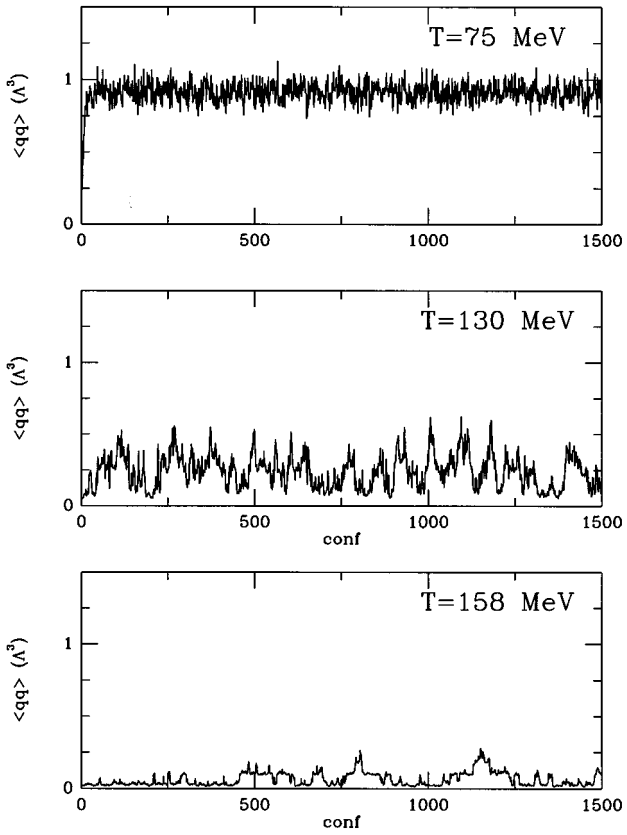


FIG. 11. Trajectories of the quark condensate at three different temperatures $T=75$, 130, and 158 meV. The quark condensate is given in units of the scale parameter.

More details of the phase transition can be inferred from the graphs in Figs. 11–13. Figure 11 shows trajectories of the quark condensate for the temperatures mentioned above. Every configuration corresponds to one complete sweep through the instanton liquid, with one Metropolis hit on the collective variables of all instantons. As discussed in more detail in the next section, the fluctuations in the quark condensate determine the scalar susceptibility. Below the phase transition, these fluctuations are controlled by the effective $\sigma$ meson mass. Near the phase transition, we find evidence for a weak first-order transition with the system frequently tunneling between the two phases. In order to clearly distinguish this scenario from a smooth crossover, we would have to run the experiment with significantly larger volumes. Figure 12 shows the spectrum of the Dirac operator. Below the phase transition, it has the familiar flat shape near the origin and extrapolates to a nonzero density of eigenvalues at $\lambda=0$. Near the phase transition, the eigenvalue density ap-

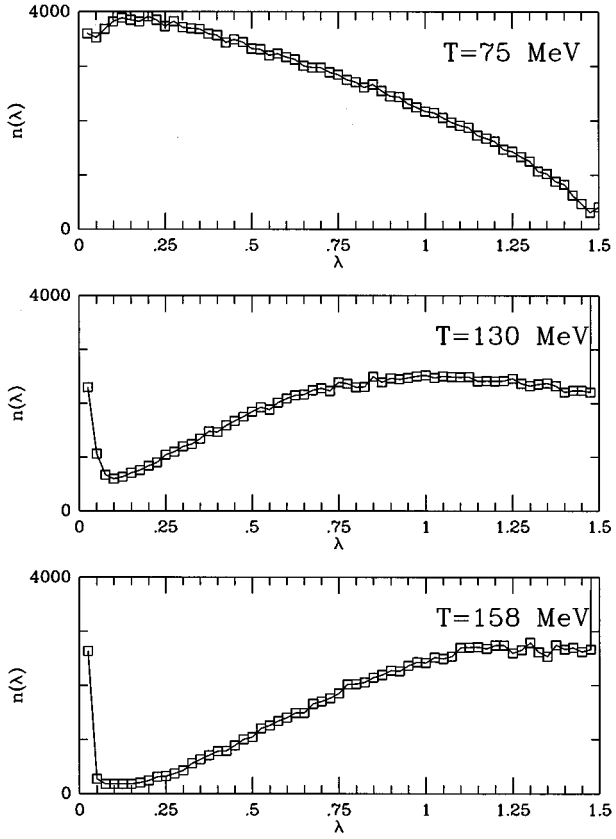


FIG. 12. Spectrum of the Dirac operator for different temperatures $T=75$, 130, and 158 MeV. The normalization of the spectra is arbitrary (but identical).

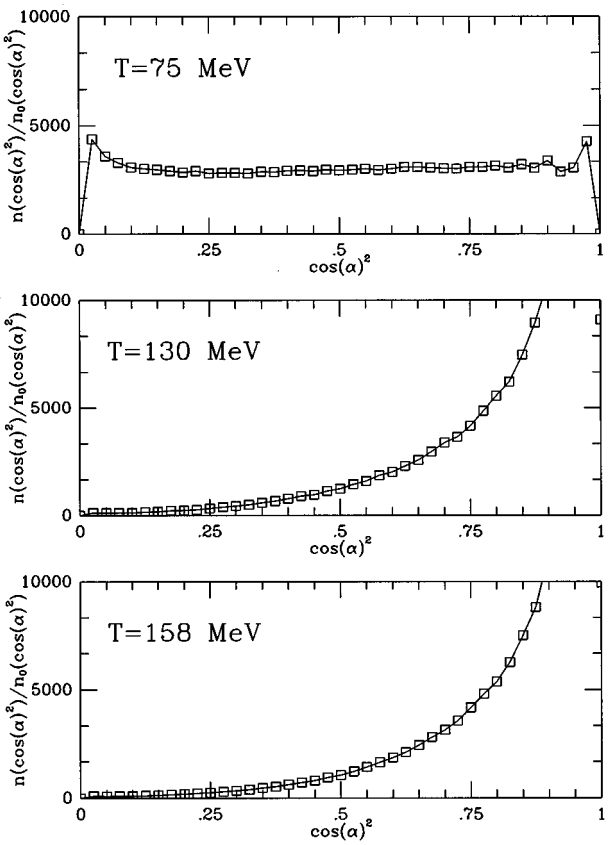


FIG. 13. Distribution of the color orientation angle $\cos^2\alpha=|u_4|^2/|u|^2$ for different temperatures $T=75$, 130, and 158 MeV. The distributions are normalized to the corresponding SU(3) measure. The overall scale is arbitrary.

pears to extrapolate to 0 at $\lambda\to 0$, but there is a spike in the eigenvalue density at $\lambda=0$. This spike contains the contribution from unpaired instantons. Near the phase transition, some of these instantons come from the breakup of molecules as the system tunnels from the high to the low temperature phase. In addition to that, even at very high temperature, one expects a finite concentration $O(m^{N_f})$ of random instantons. We will further comment on this issue in the next section.

If there is evidence that the transition is weakly first order, it is of interest to at least have an upper bound on the latent heat associated with the transition. We have already mentioned that we do not directly observe a latent heat from a discontinuity in the instanton density. Another way to calculate the latent heat is using the Clausius-Clapeyron relation generalized to QCD [65]

$$\mathrm{disc}\epsilon = T_c\left(\frac{\partial T_c}{m_q}\right)^{-1}\mathrm{disc}\langle\overline{q}q\rangle. \tag{30}$$

As Leutwyler already realized in his original paper, this relation is useful in analyzing numerical simulations even if one does not directly observe a jump in $\epsilon$. We have determined the derivative of the critical temperature with respect to the quark mass from simulations at several different quark masses (see Sec. VII). We find $\partial T_c/\partial m_q\simeq 0.9$ at $m_q=0.1\Lambda$, close to Leutwyler's estimate $\partial T_c/\partial m_q\simeq 1$. From the trajectories of the quark condensate (Fig. 11), one concludes that the discontinuity is at most $\mathrm{disc}\langle\overline{q}q\rangle\leq 0.4\langle\overline{q}q\rangle_{T=0}$. These numbers give $\mathrm{disc}\epsilon\leq 60$ MeV/fm$^3$, which is quite small as compared to the energy density at zero temperature. Saturating the trace anomaly, $(\epsilon-3p)/4=-b/4(N/V)$, with instantons, one can also translate this estimate into a bound on the jump in the instanton density, $\mathrm{disc}(N/V)\leq 0.03$ fm$^{-4}$, compared with the zero temperature value $(N/V)=1$ fm$^{-4}$. This bound shows that we do not expect to see an appreciable jump in the instanton density, even if there is a first-order transition.

In Fig. 13 we show the distribution of $\cos^2(\alpha)=|u_4|^2/|u|^2$, the relative color orientation angle between instantons and anti-instantons. For this purpose, we have selected for every instanton the anti -instanton it has the largest overlap with and calculated the corresponding orientation angle $\cos^2(\alpha)$. The resulting distribution was normalized to the SU(3)-invariant measure. Below the phase transition, there is no preferred direction and the distribution is flat [the spike near $\cos^2(\alpha)=1$ comes from the fact that the measure goes to zero in this region]. Near the phase transition, the distribution is strongly peaked towards $\cos^2(\alpha)=1$, showing that instanton–anti-instanton pairs are indeed strongly polarized.

Completing this section, let us add a few general remarks concerning the thermodynamics of the instanton liquid. In this paper, we have only determined the free energy associated with instantons. Our calculation includes the contributions from the zero-mode determinant, which describes the excitation of low energy collective modes (the pions). How-

ever, it does not include nonzero-mode contributions from quarks or gluons. In particular, it does not include the Stefan-Boltzmann contribution at large temperature, or perturbative $O(\alpha_s)$ corrections to it. In a more realistic description of the thermodynamics of the chiral phase transition, these contributions should certainly be included. (An attempt to do so was made in the schematic cocktail model by Ilgenfritz and Shuryak [31].) In this paper, however, it was our intention to study the physics contained in the partition function of the instanton liquid, without making further assumptions or inputs. Remarkably, the instanton liquid undergoes a phase transition in the expected temperature regime.

## VII. DIRAC EIGENVALUES AND MESONIC SUSCEPTIBILITIES

Beginning with the classical paper by Banks and Casher [66], many useful relations have been pointed out between various observables and the spectrum of the Dirac operator $i\hat{D}\psi_\lambda=\lambda\psi_\lambda$. In quantum field theories, the region of small $\lambda\to 0$ is the analogue of the Fermi surface in solid state physics, and understanding the density of states near this point is crucial for many properties of the system, both at zero and nonzero temperatures.

Before we discuss our data in more detail, we would like to briefly review some of the results found in the literature. As $T\to T_c$, the quark condensate vanishes. If there is a second-order phase transition for $N_f=2$, the mass dependence of the condensate is governed by the critical index $\delta$:

$$\langle\overline{qq}\rangle|_{T=T_{\max}}\sim m^{1/\delta}, \tag{31}$$

where $T_{\max}$ denotes the pseudocritical temperature, corresponding to the position of the peak in the scalar susceptibility (see below). As mentioned above, there is still some controversy concerning the values of the critical indices. According to standard universality arguments, QCD with $N_f=2$ case is analogous to the O(4) Heisenberg magnet, which has $1/\delta=0.21$. On the other hand, mean field scaling would give $1/\delta=1/3$.

Using the Banks-Casher relation,

$$\langle\overline{qq}(T)\rangle=-\int d\lambda\rho(\lambda,m,T)\frac{2m}{\lambda^2+m^2}, \tag{32}$$

one can try to convert this relation into a prediction for the spectral density of the Dirac operator. The problem is that there are two sources for the mass dependence of the condensate, the explicit mass term in the integral (the ''valence mass'') and the implicit mass dependence of the spectral density (the ''sea mass''). Combining these two effects, one can only conclude that

$$\rho(\lambda,T=T_{\max})\sim\lambda^{1/\delta-\kappa}m^{\kappa}, \tag{33}$$

where $\kappa$ characterizes the explicit mass dependence of the spectral density. Still, one may hope that the influence of the sea mass is small and study the behavior of the spectral density near zero at the phase transition. In Fig. 6 we have shown the distribution of eigenvalues at $T_c$ for the case of two flavors. The spectrum behaves roughly like $\rho(\lambda)\sim\lambda^{0.3}$. In Fig. 12 we have displayed the analogous result for QCD. Here, the spectrum consists of two parts, a smooth part behaving like $\rho(\lambda)\sim\lambda^2$ and a spike near zero. There are two effects that contribute to the spike near zero. One is the fact that near a first-order phase transition, both the broken and the restored phases contribute to the spectrum. The other is that at finite mass, there will always be a finite $O(m^{N_f})$ number of unpaired instantons, giving a contribution of the form $\rho(\lambda)\sim m^{N_f}\delta(\lambda)$ to the Dirac spectrum.

Additional information about the phase transition is provided by mesonic susceptibilities. We define these susceptibilities as the integral of the corresponding mesonic correlation function

$$\chi_\Gamma=\int d^4x\langle\overline{q}(x)\Gamma q(x)\overline{q}(0)\Gamma q(0)\rangle, \tag{34}$$

where $\Gamma$ is a spin-isospin matrix with the appropriate quantum numbers. They characterize the response of the system to slowly varying external perturbations. For example, the scalar-isoscalar susceptibility can also be defined as the second derivative of $\ln Z$ with respect to the quark mass. Near a second-order phase transition, the susceptibilities associated with order parameter fluctuations are expected to diverge in the chiral limit in a universal manner. In particular, we have the predictions [54]

$$\chi_\sigma|_{T=T_{\max}}\sim m^{1/\delta-1},\quad \left.\frac{\chi_\sigma}{\chi_\pi}\right|_{T=T_c}=1/\delta. \tag{35}$$

Above the phase transition, chiral symmetry is restored and one has $\chi_\sigma=\chi_\pi$ as the quark mass is taken to zero. Below the phase transition, $\chi_\sigma/\chi_\pi\to 0$ as $m\to 0$, since $\chi_\pi$ has a $1/m$ singularity in the chiral limit, while $\chi_\sigma$ only has a logarithmic singularity. As noted by Karsch and Laermann [56], the second relation in (35) is very useful in determining the exponent $\delta$, since measurements of $\Delta(m,T)=\chi_\sigma/\chi_\pi$ at different masses are expected to cross at a unique temperature $T=T_c$, where the value of $1/\delta$ can be extracted from $\Delta(m,T_c)$ (up to corrections from the nonsingular part of the free energy).

The susceptibilities associated with flavored mesons like the $\pi$ and $\delta$ meson are directly related to the spectrum of the Dirac operator. Inserting the general decomposition of the quark propagator in terms of eigenfunctions into the definition (34), one finds

$$\chi_\pi=2\int d\lambda\rho(\lambda,mT)\frac{1}{\lambda^2+m^2}, \tag{36}$$

$$\chi_\delta=2\int d\lambda\rho(\lambda,m,T)\frac{\lambda^2-m^2}{(\lambda^2+m^2)^2}. \tag{37}$$

Comparing (36) with the Banks-Casher relation (32), one notes that $\chi_\pi=-\langle\overline{qq}\rangle/m$, a relation that can also be obtained by saturating the pion correlator with one-pion intermediate states and using PCAC (partial conservation of axial

vector current). The susceptibility in the scalar-isoscalar ($\sigma$ meson) channel receives an additional contribution from disconnected diagrams, which cannot be expressed in terms of the spectral density

$$\chi_\sigma = \chi_\delta + 2V[\langle(\langle\overline{q}q\rangle)^2\rangle - \langle\overline{q}q\rangle^2]. \tag{38}$$

The second term measures the fluctuations of the quark condensate in a finite volume $V$ (as the volume is taken to infinity). Note that all the susceptibilities (36)–(38) suffer from ultraviolet divergencies related to the behavior of $\rho(\lambda)$ at large $\lambda$. The critical behavior, on the other hand, is determined by the spectrum at small virtuality. In the following, we will evaluate the susceptibilities in the zero mode basis.

One important aspect of the QCD phase transition is the question whether the $U(1)_A$ symmetry is restored during the transition [67]. If this is the case, one expects (for $N_f=2$) two additional degrees of freedom to become light during the transition, the $\eta'$ and $\delta$. The $\eta'$ susceptibility is connected with fluctuations of the number of zero modes of the Dirac operator and cannot be measured directly in a system with total topological charge zero.[7] The $\delta$ susceptibility, however, can easily be studied in our simulations. If $U(1)_A$ symmetry is restored, we expect $\chi_\delta$ to peak at the transition and diverge as the quark mass is taken to zero. Furthermore, above the transition, one would have[8] $\chi_\pi = \chi_\delta$ as $m \to 0$. This also requires that the disconnected part of $\chi_\sigma$ has to vanish for $T > T_c$ as $m \to 0$.

We show our results for the mesonic susceptibilities in Figs. 14 and 15. The results in Fig. 14 were obtained for three flavors with masses $m_u = m_d = 0.10\Lambda = 22$ MeV and $m_s = 0.70\Lambda = 155$ MeV, corresponding to the instanton density and free energy discussed in the last section. The susceptibilities were obtained from 1000 configurations separated by five sweeps through an ensemble of 64 instantons. In our simulations, the physical volume depends on the temperature, since the number of instantons is held fixed while their density drops with temperature. Near the phase transition, we have $V_3 = (3.5 \text{ fm})^3$. In Fig. 15 we show our results for a slightly smaller light quark mass $m_u = m_d = 0.07\Lambda = 15$ MeV.

Figure 14 clearly shows a peak in the sigma susceptibility, indicating the chiral phase transition. The position of the peak is at $T \simeq 125$ MeV, somewhat too low as compared to the estimate $T_c = 140$ MeV from lattice simulations. The delta susceptibility does not show any pronounced enhancement. This is also seen from the lower part of the figure, where we show the disconnected part of the scalar susceptibility and the difference $\chi_\pi - \chi_\delta$. Clearly, the peak in $\chi_\sigma$ comes completely from the disconnected part. Furthermore, $\chi_\pi - \chi_\delta$ becomes very small above the phase transition, but shows no tendency to go to zero in the range of temperatures studied. At the smaller mass (see Fig. 15), there is a broad

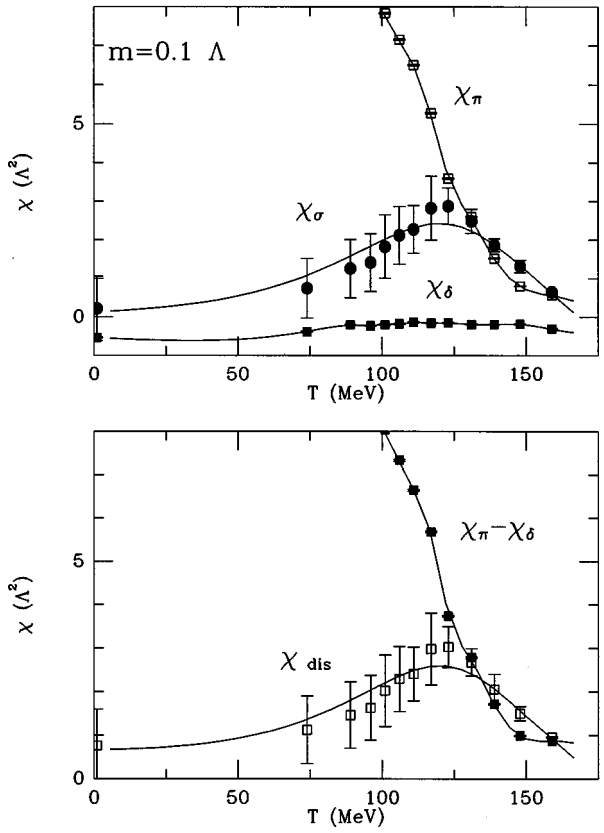


FIG. 14. Mesonic susceptibilities as a function of temperature for quark masses $m_u = m_d = 0.10\Lambda$ and $m_s = 0.70\Lambda$. The scalar $\sigma$, scalar $\delta$, and pseudoscalar $\pi$ susceptibilities are denoted by solid circles, solid squares, and open squares, respectively. The lower panel shows the disconnected part of the scalar susceptibility and the difference $\chi_\pi - \chi_\delta$. The solid lines show a smooth fit to the data.

enhancement visible in $\chi_\delta$ and $\chi_\pi - \chi_\delta$ appears to vanish above the phase transition. On the other hand, if one compares the peak heights of $\chi_\sigma$ for the two different quark masses, one finds $\chi_{\sigma,\max} \sim m^{-1.9}$, significantly stronger than the $(N_f=2)$ universality prediction. In addition to that, if one calculates the chiral cumulants $\Delta(m,T) = \chi_\sigma/\chi_\pi$ for the two different masses, they fail to cross in the regime of temperatures studied.

This may be an indication that the quark mass $m = 0.07\Lambda$ is already too small and one is entering the regime of ''mesoscopic'' QCD, where the mass is smaller or comparable to the smallest eigenvalue $\lambda_{\min} = O(1/V)$ of the Dirac operator. There is now a well-developed theory of this regime [38,68], which we do not want to enter here. Instead, we have extended our calculations to larger masses $m_u = m_d = (0.10, 0.13, 0.15, 0.17)\Lambda$. In Fig. 16 we show the maximum in the disconnected part of the scalar susceptibility as a function of the quark mass. For $m \geq 0.10\Lambda$, the behavior is well described by a single exponent. Fitting the dependence of the peak height on the light quark mass, we find $\chi_{\text{dis},\max} \sim m^{-0.84}$, quite consistent with the $(N_f=2)$ universality prediction $\chi_{\sigma,\max} \sim m^{-0.79}$.

[7] It was demonstrated in [21] that one can study the topological susceptibility by studying fluctuations of the topological charge in subvolumes of a large system with total charge zero.

[8] We are grateful to N. Christ for pointing this out.

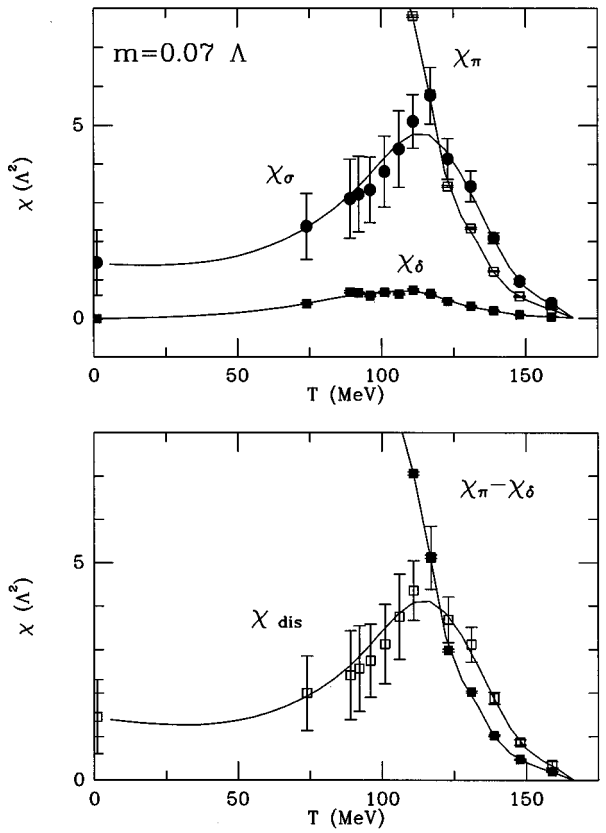


FIG. 15. Mesonic susceptibilities for a smaller light quark mass $m_u = m_d = 0.07\Lambda$. Curves labeled as in Fig. 14.

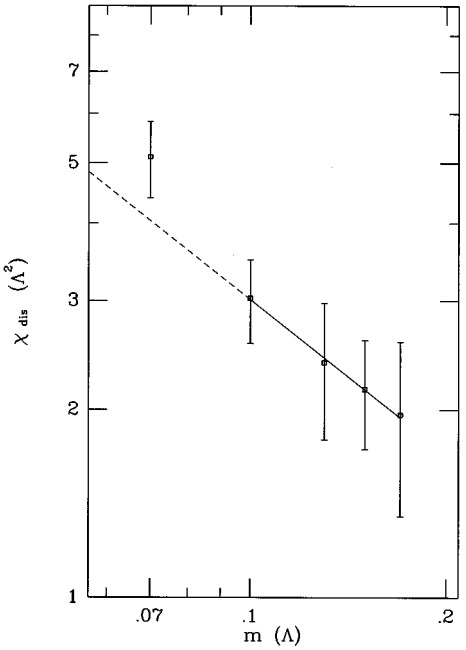


FIG. 16. Maximum of the disconnected part of the scalar susceptibility as a function of the quark mass. Also shown is the parametrization $\chi \sim m^{-0.84}$.

## VIII. CONCLUSIONS

We have studied the structure of the instanton liquid at zero and finite temperatures. For this purpose, we have introduced a method that allows us to extract the free energy of the instanton liquid from numerical simulations. Using this method, we can determine the instanton density self-consistently, by minimizing the free energy. The resulting ensemble satisfies a number of important nonperturbative properties of QCD, such as the trace anomaly, low energy theorems for fluctuations of the topological charge and gluonic field strength and chiral perturbation theory predictions for the spectrum of the Dirac operator. These features do not depend on details of the instanton interaction, as long as it is sufficiently repulsive at short distances to stabilize the system.

If we supplement the classical streamline interaction by a short range repulsive core (roughly determined to give the correct average instanton size), the instanton liquid in full QCD (with two light and one intermediate mass flavors) stabilizes at a density $N/V = 0.174\Lambda^4$. Fixing the scale parameter in order to reproduce the ''canonical'' value $N/V = 1$ fm$^4$ [corresponding to $\langle(\alpha_s/\pi)G^2\rangle = (360\ \text{MeV})^4$], we find a vacuum energy density $\epsilon = -280$ MeV/fm$^3$ and a quark condensate $\langle\overline{q}q\rangle = -(216\ \text{MeV})^3$. The average instanton size is $\rho = 0.43$ fm, leading to a packing fraction $f = 0.5\pi^2\rho^4/(N/V) = 0.14$.

This means that the interacting instanton ensemble, especially using the ratio *Ansatz* required at finite temperature, is not as dilute as the random ensemble (where we fixed $N/V = 1$ fm$^{-4}$ and $\rho = 0.33$ fm), which so successfully reproduces many hadronic correlation functions. The situation is quite analogous to the nuclear matter problem, where reproducing the saturation density and the binding energy requires a delicate balance between the short range repulsive core and the intermediate range attraction. In the instanton liquid, the strength of the core (the short range repulsion) controls the diluteness of the ensemble. Too much repulsion, however, leads to a very small total density of instantons, which can only be balanced by some intermediate range attraction. In the ratio *Ansatz*, the short range core is weak and the intermediate range attraction fairly shallow, leading to a rather dense ensemble.

We note that at this point, the instanton–anti-instanton interaction at short distances is not a very well-defined concept, and the core that is required to stabilize the ensemble (for the streamline *Ansatz*) is a purely phenomenological parameter. In practice, we have fixed this parameter in order to reproduce the instanton density and size distribution inferred from phenomenologial considerations and observed in lattice simulations [17,18]. Providing a more solid theoretical foundation for the instanton interaction will be an important direction for future study. One possibility, to derive the short range part of the instanton interaction from the cross section for isotropic multigluon production [44], was already mentioned in Sec. IV. Another idea, the inclusion of nonperturbative corrections to the beta function, was discussed in [19].

We have extended our simulations of the instanton liquid to finite temperature. For this purpose, we have to replace the instanton interaction and fermionic overlap matrix elements with their finite temperature counterparts, satisfying the appropriate boundary conditions in an Euclidean box with temporal extent $1/T$. In this context, we have used the ratio *Ansatz*, which gives an ensemble that is too dense. This brings some additional uncertainty into our numerical re-

sults, e.g., of the transition temperature. We find that in full QCD, there is a phase transition at $T \simeq 125$ MeV in which the chiral symmetry is restored. The mechanism that drives the transition is the formation of polarized instanton–anti-instanton molecules. As a result, the (quasi-)zero-modes become localized, and chiral symmetry is restored.

Furthermore, for two light flavors the transition appears to be second order, while for $N_f \geq 3$, there is evidence for a weak first-order transition. We have also investigated the phase diagram of QCD with many fermion flavors. Qualitatively, it is clear that many fermion flavors help the formation of molecules. As a result, the transition temperature drops as the number of light flavors is increased. For $N_f$ larger than some critical value $N_f^{\rm crit}$, chiral symmetry is restored even at zero temperature. For $N_c = 2,3$, our results are consistent with $N_f^{\rm crit} = N_c + C$, where $1 < C < 2$. We have also studied the location of the discontinuity of the quark condensate in the $T$-$m$ plane.

We have determined the free energy associated with instantons, ignoring the perturbative (nonzero-mode) contributions from quarks and gluons. At small $T$, it rises slightly, but then starts to drop and becomes very small for $T > 180$ MeV. While the energy density and pressure above $T_c$ are dominated by the perturbative Stefan-Boltzmann contributions, instantons can provide a significant contribution to the so called ''interaction measure'' $B = -(\epsilon - 3p)/4$ even at $T > T_c$. Apart from the location of the phase transition, the most important result of our work is that $B$ retains about half of its $T = 0$ value at $T = T_c$. Using the trace anomaly, the interaction measure is related to the gluon and quark condensates. Indeed, by analyzing lattice simulations of full QCD, one can show that about half of the glue remains condensed at $T = T_c$ [69–71]. More specifically, lattice simulations show that the pressure remains small until $T \simeq 2T_c$, while the energy density reaches the Stefan-Boltzmann value very quickly [41,72,57]. It was emphasized in [69] that this behavior requires that only part of the bag pressure (or the gluon condensate) is removed across the phase transition. This is precisely the behavior observed in the instanton liquid model.

Finally, we have studied the behavior of the Dirac spectrum and the mesonic susceptibilities near the phase transition. This is related to the question whether the behavior of these quantities is governed by critical scaling because of a nearby second-order phase transition, and, more generally, what symmetries are restored in the transition. We find a peak in the scalar-isoscalar ($\sigma$) susceptibility, indicating the chiral phase transition. The dependence of the peak height on the light quark mass is consistent with the expected scaling behavior at fairly large quark masses $m \geq 0.1\Lambda$, but is more singular at smaller masses, probably due to the onset of finite-size effects. For $m \geq 0.1\Lambda$, there is no hint of $\mathrm{U}(1)_A$ restoration: there is no peak in the isovector scalar ($\delta$) susceptibility and the Dirac spectrum contains (approximately) zero modes above $T_c$. At smaller masses, the scalar-isovector ($\delta$) susceptibility shows an enhancement around the critical point, but with the available data it is difficult to tell whether this behavior will persist for larger volumes.

## ACKNOWLEDGMENTS

We would like to thank J. J. M. Verbaarschot for many useful discussions. We have also benefited from conversations with A. Smilga and I. Zahed. Part of this work was done while T.S. was a visitor at the Institute for Nuclear Theory in Seattle. The reported work was partially supported by the U.S. DOE Grant No. DE-FG-88ER40388. Most of the numerical calculations were performed at the NERSC at Lawrence Livermore.

## APPENDIX A: INSTANTON INTERACTION AT ZERO TEMPERATURE

In this appendix we specify the classical instanton interaction used in our simulations. From the form of the action for the two-instanton *Ansatz*, one can easily show that the general form of the instanton–anti-instanton interaction in the case of the gauge-group SU(2) is given by

$$S_{\rm int} = \beta_1(\overline{\rho})(s_0(R) + s_1(R)(u\cdot\hat{R})^2 + s_2(R)(u\cdot\hat{R})^4), \quad \text{(A1)}$$

where $u_\mu$ is the orientation vector introduced in Sec. II and $\hat{R}_\mu$ is the unit vector connecting the centers of the instanton and anti-instanton. The interaction is given in units of the single instanton action $S_0 = \beta_1(\overline{\rho})$. The argument of the beta function is not uniquely determined without a higher order calculation. In practice, we have taken the geometric average $\overline{\rho} = \sqrt{\rho_I \rho_A}$ of the instanton radii. For large separation $R$, the interaction (A1) can be embedded into SU(3) by making the replacement $(u\cdot\hat{R})^2 \to |u\cdot\hat{R}|^2$ and multiplying the first term by $|u|^2$.

For the ratio *Ansatz*, the instanton–anti-instanton interaction can be parametrized by [52]

$$\frac{S_{IA}}{\beta_1} = \left(\frac{4.0}{(r^2+2.0)^2} - \frac{1.66}{(1+1.68r^2)^3} + \frac{0.72\,\ln(r^2)}{(1+0.42r^2)^4}\right)|u|^2 + \left(-\frac{16.0}{(r^2+2.0)^2} + \frac{2.73}{(1+0.33r^2)^3}\right)|u\cdot\hat{R}|^2, \quad \text{(A2)}$$

where $r = R/\sqrt{\rho_I \rho_A}$ is the instanton–anti-instanton separation in units of the geometric mean of their radii. In the ratio *Ansatz*, the instanton-instanton interaction is nonzero if the two instantons have different color orientations. The interaction can be parametrized by

$$\frac{S_{II}}{\beta_1} = \frac{1}{(1+0.43r^2)^3}[0.63|\vec{u}|^2 + 0.071|\vec{u}|^4] - \frac{\ln(r^2)}{(1+1.17r^2)^4}[0.05|\vec{u}|^2 + 0.47|\vec{u}|^4]. \quad \text{(A3)}$$

In the streamline *Ansatz*, conformal symmetry dictates that the interaction depends on the relative separation and the instanton radii only through the conformal parameter

$$\lambda = \frac{R^2 + \rho_I^2 + \rho_A^2}{2\rho_I\rho_A} + \left(\frac{(R^2+\rho_I^2+\rho_A^2)^2}{4\rho_I^2\rho_A^2} - 1\right)^{1/2}. \quad \text{(A4)}$$

The instanton–anti-instanton interaction is then given by [35]

$$\frac{S_{IA}}{\beta_1}=\frac{4}{(\lambda^2-1)^3}\{-4[1-\lambda^4+4\lambda^2\ln(\lambda)][|u|^2-4|u\cdot\hat{R}|^2]$$
$$+2[1-\lambda^2+(1+\lambda^2)\ln(\lambda)][(|u|^2-4|u\cdot\hat{R}|^2)^2$$
$$+|u|^4+2(u)^2(u^*)^2]\}. \quad \text{(A5)}$$

As discussed in Sec. II, the instanton-instanton interaction vanishes in the streamline *Ansatz*.

## APPENDIX B: FERMIONIC OVERLAP MATRIX ELEMENTS AT ZERO TEMPERATURE

A parametrization of the fermionic overlap matrix element between instantons and anti-instantons in the sum *Ansatz* was already given in Sec. II:

$$T_{IA}=i(u\cdot R)\frac{1}{\rho_I\rho_A}\frac{4.0}{(2.0+R^2/\rho_I\rho_A)^2}. \quad \text{(B1)}$$

The matrix element in the ratio *Ansatz* is very similar and we employ the same parametrization. In the streamline *Ansatz*, the matrix element depends on the separation and the radii again only through the conformal parameter $\lambda$. The matrix element can be parametrized by [73]

$$T_{IA}=i(u\cdot R)\frac{1}{\rho_I\rho_A}\frac{c_1\lambda^{3/2}}{[1+1.25(\lambda^2-1)+c_2(\lambda^2-1)^2]^{3/4}}, \quad \text{(B2)}$$

with $c_1=3\pi/8$ and $c_2=(3\pi/32)^{4/3}$.

## APPENDIX C: INSTANTON INTERACTION AT FINITE TEMPERATURE

In this appendix we give a parametrization of the classical instanton interaction at finite temperature. For reasons explained in Sec. IV, there is no analogue of the streamline interaction at finite temperature and we only specify the interaction in the ratio *Ansatz*. Up to small changes that have been introduced in order to improve the parametrization at small temperatures, the interaction is identical to the one given in [52]. Here, we also specify how to embed the SU(2) parametrization into SU(3).

At finite temperature, the interaction is still at most quartic in the relative orientation vector $u_\mu$. However, since four-dimensional rotational invariance is broken, the interaction depends on $|u_4|^2$ in addition to the invariants $|u\cdot\hat{R}|^2$ and $|u|^2$ appearing in the zero temperature interaction. For the same reason, the interaction can now depend separately on the spatial and temporal components of the vector $R_\mu=(\vec{R},R_4)$. At temperatures of interest here, the anisotropy in the dependence of $R_\mu$ turns out to be small. The parametrization

$$\frac{S_{IA}}{\beta_1}=\frac{4.0}{(r^2+2.0)^2}\frac{\beta^2}{\beta^2+5.21}|u|^2-\left(\frac{1.66}{(1+1.68r^2)^3}+\frac{0.72\,\ln(r^2)}{(1+0.42r^2)^4}\right)\frac{\beta^2}{\beta^2+0.75}|u|^2$$
$$+\left(-\frac{16.0}{(r^2+2.0)^2}+\frac{2.73}{(1+0.33r^2)^3}\right)\frac{\beta^2}{\beta^2+0.24+11.50r^2/(1+1.14r^2)}|u\cdot\hat{R}|^2$$
$$+0.36\,\ln\left(1+\frac{\beta}{r}\right)\frac{1}{(1+0.013r^2)^4}\frac{1}{\beta^2+1.73}(|u|^2-|u\cdot\hat{R}|^2-|u_4|^2) \quad \text{(C1)}$$

therefore depends only on $r=R/\sqrt{\rho_I\rho_A}$ with $R=(\vec{R}^2+R_4^2)^{1/2}$. The inverse temperature $\beta=1/(T\sqrt{\rho_I\rho_A})$ is also given in units of the mean of the instanton radii. One can easily check that for $T\to 0$, the interaction (C1) reduces to the zero temperature ratio *Ansatz* (A2). The interaction between two instantons can be parametrized by

$$\frac{S_{II}}{\beta_1}=\frac{1}{(1+0.43r^2)^3}\frac{\beta^2}{\beta^2+5.33}[0.63|\vec{u}|^2+0.071|\vec{u}|^4]-\frac{\ln(r^2)}{(1+1.17r^2)^4}\frac{\beta^2}{\beta^2+1.17}[0.05|\vec{u}|^2+0.47|\vec{u}|^4]$$
$$+\ln\left(1+\frac{\beta}{r}\right)\frac{1}{\beta^2+2.08}[0.07|\vec{u}|^2+0.05|\vec{u}|^4]. \quad \text{(C2)}$$

## APPENDIX D: FERMIONIC OVERLAP MATRIX ELEMENTS AT FINITE TEMPERATURE

At finite temperature, the fermionic overlap matrix element is still linear in the relative orientation vector $u_\mu$. Because of the loss of Lorentz invariance at finite temperature, the matrix element depends separately on $u_4$ and $\vec{u}\cdot\vec{R}$:

$$T_{IA}=iu_4f_1+i\frac{(\vec{u}\cdot\vec{R})}{R}f_2. \quad \text{(D1)}$$

A parametrization of the functions $f_{1,2}$ was given in [52]. We have changed this parametrization slightly in order to improve the behavior at small temperatures. The result for $f_1$ is

$$f_1=\frac{\left(\frac{\pi}{\beta}\right)\sin\left(\frac{\pi\tau}{\beta}\right)\cosh\left(\frac{\pi r}{\beta}\right)}{\left[\cosh\left(\frac{\pi r}{\beta}\right)-\cos\left(\frac{\pi\tau}{\beta}\right)+\kappa_1^2\right]^2}\frac{1}{\left(\frac{\beta^2}{\pi^2}\right)\left[\exp\left(-\frac{\pi r}{2\beta}\right)+\frac{\pi r}{2\beta}\right]+\left(\frac{2}{\pi}\right)\left[1-0.69\,\exp\left(-\frac{1.75r}{\beta}\right)\right]}$$
$$\times\left(1+\frac{0.76\beta^2}{(0.82r^2+1)^2(1+0.19\beta^2)^2}\right)\left[1+\left(\frac{\pi\tau}{\beta}\right)^2\frac{0.18}{1+0.12r^2}\right], \tag{D2}$$

where $r=|\vec{R}|/\sqrt{\rho_I\rho_A}$, $\tau=R_4/\sqrt{\rho_I\rho_A}$, and $\beta=1/(T\sqrt{\rho_I\rho_A})$ are given in units of the mean instanton radius. The result for $f_2$ is

$$f_2=\frac{\left(\frac{\pi}{\beta}\right)\cos\left(\frac{\pi\tau}{\beta}\right)\sinh\left(\frac{\pi r}{\beta}\right)}{\left[\cosh\left(\frac{\pi r}{\beta}\right)-\cos\left(\frac{\pi\tau}{\beta}\right)+\kappa_2^2\right]^2}\frac{1}{\left(\frac{\beta^2}{\pi^2}\right)\left[\exp\left(-\frac{2.06\pi r}{\beta}\right)+\frac{\pi r}{2\beta}\right]+\left(\frac{2}{\pi}\right)\left[1+0.42\,\exp\left(-\frac{0.34r}{\beta}\right)\right]}, \tag{D3}$$

with $\kappa_{1,2}$ given by

$$\kappa_1^2=\frac{1}{0.53+\left(\frac{\beta^2}{\pi^2}\right)},\quad \kappa_2^2=\frac{1}{0.69+\left(\frac{\beta^2}{\pi^2}\right)}. \tag{D4}$$

One can easily verify that the parametrization (D1)–(D4) reduces to (B1) in the zero temperature limit.


[1] A. A. Belavin, A. M. Polyakov, A. S. Schwartz, and Y. S. Tyupkin, Phys. Lett. **59B**, 85 (1975).
[2] G. 't Hooft, Phys. Rev. D **14**, 3432 (1976).
[3] C. G. Callan, R. Dashen, and D. J. Gross, Phys. Rev. D **17**, 2717 (1978).
[4] E. V. Shuryak, Phys. Lett. **79B**, 135 (1978).
[5] M. A. Shifman, A. I. Vainshtein, and V. I. Zakharov, Nucl. Phys. **B147**, 385 (1979).
[6] E. V. Shuryak, Nucl. Phys. **B203**, 93 (1982); **B203**, 116 (1982).
[7] D. I. Diakonov and V. Yu. Petrov, Nucl. Phys. **B245**, 259 (1984).
[8] E. M. Ilgenfritz and M. Müller-Preussker, Nucl. Phys. **B184**, 443 (1981).
[9] E. V. Shuryak, Nucl. Phys. **B302**, 559 (1988); **B302**, 574 (1988); **B302**, 599 (1988).
[10] E. V. Shuryak, Nucl. Phys. **B319**, 521 (1989); **B319**, 541 (1989).
[11] E. V. Shuryak and J. J. M. Verbaarschot, Nucl. Phys. **B410**, 55 (1993); T. Schäfer, E. V. Shuryak, and J. J. M. Verbaarschot, *ibid.* **B412**, 143 (1994).
[12] T. Schäfer and E. V. Shuryak, Phys. Rev. D **50**, 478 (1994).
[13] T. Schäfer and E. V. Shuryak, Phys. Rev. Lett. **75**, 1707 (1995).
[14] E. V. Shuryak, Rev. Mod. Phys. **65**, 1 (1993).
[15] M. C. Chu, J. M. Grandy, S. Huang, and J. W. Negele, Phys. Rev. Lett. **70**, 225 (1993); Phys. Rev. D **48**, 3340 (1993).
[16] B. Berg, Phys. Lett. **B114**, 475 (1981); M. Teper, in *Lattice '90*, Proceedings of the International Symposium, Tallahassee, Florida, edited by V. A. Iteller, A. D. Kennedy, and S. Sanielevici [Nucl. Phys. B (Proc. Suppl.) **20**, 159 (1991)].
[17] M. C. Chu, J. M. Grandy, S. Huang, and J. W. Negele, Phys. Rev. D **49**, 6039 (1994).
[18] C. Michael and P. S. Spencer, Phys. Rev. D **50**, 7570 (1994); **52**, 4691 (1995).
[19] E. V. Shuryak, Phys. Rev. D **52**, 5370 (1995).
[20] T. Schäfer and E. V. Shuryak, Stony Brook Report No. SUNY-NTG-95-23 (unpublished).
[21] E. V. Shuryak and J. J. M. Verbaarschot, Phys. Rev. D **52**, 295 (1995).
[22] I. Zahed, Nucl. Phys. **B427**, 561 (1994).
[23] D. I. Diakonov and A. D. Mirlin, Phys. Rev. B **203**, 299 (1988).
[24] M. A. Nowak, J. J. M. Verbaarschot, and I. Zahed, Nucl. Phys. **B325**, 581 (1989).
[25] R. D. Pisarski and L. G. Yaffe, Phys. Lett. **97B**, 110 (1980); D. J. Gross, R. D. Pisarski, and L. G. Yaffe, Rev. Mod. Phys. **53**, 43 (1981).
[26] E.-M. Ilgenfritz and E. V. Shuryak, Nucl. Phys. **B319**, 511 (1989).
[27] V. Khoze and A. Yung, Z. Phys. C **50**, 155 (1991).
[28] E. V. Shuryak and M. Velkovsky, Phys. Rev. D **50**, 3323 (1994).
[29] M. C. Chu and S. Schramm, Phys. Rev. D **51**, 4580 (1995).
[30] E.-M. Ilgenfritz, M. Müller-Preussker, and E. Meggiolaro, in *Lattice '94*, Proceedings of the International Symposium, Bielefeld, Germany, edited by F. Karsch *et al.* [Nucl. Phys. B (Proc. Suppl.) **42**, 496 (1995)].
[31] E.-M. Ilgenfritz and E. V. Shuryak, Phys. Lett. B **325**, 263 (1994).
[32] T. Schäfer, E. V. Shuryak, and J. J. M. Verbaarschot, Phys. Rev. D **51**, 1267 (1995).

[33] T. Schäfer and E. V. Shuryak, Phys. Lett. B **356**, 147 (1995).
[34] A. V. Yung, Nucl. Phys. **B297**, 47 (1988).
[35] J. J. M. Verbaarschot, Nucl. Phys. **B362**, 33 (1991).
[36] D. I. Diakonov and V. Yu. Petrov, Nucl. Phys. **B272**, 457 (1986).
[37] M. A. Shifman, A. I. Vainshtein, and V. I. Zakharov, Nucl. Phys. **B163**, 43 (1980).
[38] H. Leutwyler and A. Smilga, Phys. Rev. D **46**, 5607 (1992).
[39] E. V. Shuryak and J. J. M. Verbaarschot, Nucl. Phys. **B341**, 1 (1990).
[40] E. V. Shuryak and O. V. Zhirov, Nucl. Phys. **B242**, 393 (1984).
[41] J. Engels, J. Fingberg, F. Karsch, D. Miller, and M. Weber, Phys. Lett. B **252**, 625 (1990); T. Blum, L. Kärkkäinnen, D. Toussaint, and S. Gottlieb, Phys. Rev. D **51**, 5133 (1995).
[42] E. V. Shuryak, Phys. Lett. **153B**, 162 (1985).
[43] D. I. Diakonov and V. Yu. Petrov, Sov. Phys. JETP **89**, 361 (1985); Phys. Lett. **147B**, 357 (1984).
[44] D. I. Diakonov and V. Yu. Petrov, Nucl. Phys. **B389**, 109 (1991).
[45] D. I. Diakonov and V. Yu. Petrov, Phys. Rev. D **50**, 266 (1994).
[46] V. A. Novikov, M. A. Shifman, A. I. Vainshtein, and V. I. Zakharov, Nucl. Phys. **B165**, 67 (1979).
[47] M. A. Nowak, J. J. M. Verbaarschot, and I. Zahed, Phys. Lett. B **228**, 115 (1989).
[48] A. Smilga and J. Stern, Phys. Lett. B **318**, 531 (1993).
[49] N. Dowrick and M. Teper, in *Lattice '94* [30], p. 237.
[50] J. J. M. Verbaarschot, Acta. Phys. Pol. **25**, 133 (1994); Nucl. Phys. **B427**, 534 (1994).
[51] B. J. Harrington and H. K. Shepard, Phys. Rev. D **17**, 2122 (1978); B. Grossman, Phys. Lett. **61A**, 86 (1977).
[52] E. V. Shuryak and J. J. M. Verbaarschot, Nucl. Phys. **B364**, 255 (1991).
[53] R. D. Pisarski and F. Wilczek, Phys. Rev. D **29**, 338 (1984).
[54] F. Wildzek, Int. J. Mod. Phys. A **7**, 3911 (1992); K. Rajagopal, and F. Wilczek, Nucl. Phys. **B399**, 395 (1993).
[55] A. Kocic and J. Kogut, Phys. Rev. Lett. **74**, 3109 (1995); Nucl. Phys. **B455**, 229 (1995).
[56] F. Karsch and E. Laermann, Phys. Rev. D **50**, 6954 (1994).
[57] C. DeTar, in *Quark Gluon Plasma 2*, edited by R. Hwa (World Scientific, Singapore, 1995).
[58] T. Banks and A. Zaks, Nucl. Phys. **B82**, 196 (1982).
[59] E. V. Shuryak, Phys. Lett. B **196**, 373 (1987).
[60] Y. Iwasaki, K. Kanaya, S. Sakai, and T. Yoshie, in *Lattice '93*, Proceedings of the International Symposium, Dallas, Texas, edited by T. Draper *et al.* [Nucl. Phys. B (Proc. Suppl.) **34**, 314 (1994)].
[61] N. Christ, in *Lattice '92*, Proceedings of the International Symposium, Amsterdam, The Netherlands, edited by J. Smit and P. van Baal [Nucl. Phys. B (Proc. Suppl.) **30**, 323 (1993)].
[62] N. Seiberg, Phys. Rev. D **49**, 6857 (1994).
[63] S. Chandrasekharan, in *Lattice '94* [30], p. 475.
[64] J. Engels, F. Karsch, and H. Satz, Nucl. Phys. **B315**, 419 (1989).
[65] H. Leutwyler, Phys. Lett. B **284**, 106 (1992).
[66] T. Banks and A. Casher, Nucl. Phys. **B169**, 103 (1980).
[67] E. V. Shuryak, Comments Nucl. Part Phys. **21**, 235 (1994).
[68] J. J. M. Verbaarschot and I. Zahed, Phys. Rev. Lett. **70**, 3852 (1993); J. J. M. Verbaarschot, *ibid.* **72**, 2531 (1994).
[69] V. Koch and G. E. Brown, Nucl. Phys. **A560**, 345 (1993).
[70] Y. Deng, in *Lattice '88*, Proceedings of the International Symposium, Batavia, Illinois, edited by A. S. Kronfeld and P. B. Mackenzie [Nucl. Phys. B (Proc. Suppl.) **9**, 334 (1989)].
[71] C. Adami, T. Hatsuda, and I. Zahed, Phys. Rev. D **43**, 921 (1991).
[72] J. B. Kogut, D. K. Sinclair, and K. C. Wang, Phys. Lett. B **263**, 101 (1991).
[73] E. V. Shuryak and J. J. M. Verbaarschot, Phys. Rev. Lett. **68**, 2576 (1992).